Title
Targeted ablation of Crb2 in photoreceptor cells induces retinitis pigmentosa

Journal
Human Molecular Genetics, 23(13)

ISSN
0964-6906

Authors
Alves, Celso Henrique
Pellissier, Lucie P
Vos, Rogier M
et al.

Publication Date
2014-07-01

DOI
10.1093/hmg/ddu048

Peer reviewed

Human Molecular Genetics, 2014, Vol. 23, No. 13 **3384–3401**
doi:10.1093/hmg/ddu048
Advance Access published on February 2, 2014

Targeted ablation of *Crb2* in photoreceptor cells induces retinitis pigmentosa

Celso Henrique Alves[1], Lucie P. Pellissier[1], Rogier M. Vos[1], Marina Garcia Garrido[4], Vithiyanjali Sothilingam[4], Christina Seide[4], Susanne C. Beck[4], Jan Klooster[2], Takahisa Furukawa[5,6], John G. Flannery[7], Joost Verhaagen[3], Mathias W. Seeliger[4] and Jan Wijnholds[1,*]

[1]Department of Neuromedical Genetics, [2]Department of Retinal Signal Processing and [3]Department of Neuroregeneration, The Netherlands Institute for Neuroscience, Royal Netherlands Academy of Arts and Sciences (KNAW), Meibergdreef 47, 1105 BA Amsterdam, The Netherlands, [4]Division of Ocular Neurodegeneration, Institute for Ophthalmic Research, Centre for Ophthalmology, Eberhard Karls University of Tübingen, Tübingen D-72076, Germany, [5]Institute for Protein Research & CREST-JST, Osaka University, Osaka, Japan, [6]Department of Developmental Biology, Osaka Bioscience Institute, Suita, Osaka, Japan and [7]Department of Molecular and Cellular Biology and The Helen Wills Neuroscience Institute, University of California, Berkeley, CA, USA

Received December 13, 2013; Revised and Accepted January 29, 2014

In humans, the Crumbs homolog-1 (*CRB1*) gene is mutated in autosomal recessive Leber congenital amaurosis and early-onset retinitis pigmentosa. In mammals, the Crumbs family is composed of: CRB1, CRB2, CRB3A and CRB3B. Recently, we showed that removal of mouse *Crb2* from retinal progenitor cells, and consequent removal from Müller glial and photoreceptor cells, results in severe and progressive retinal degeneration with concomitant loss of retinal function that mimics retinitis pigmentosa due to mutations in the *CRB1* gene. Here, we studied the effects of cell-type-specific loss of CRB2 from the developing mouse retina using targeted conditional deletion of *Crb2* in photoreceptors or Müller cells. We analyzed the consequences of targeted loss of CRB2 in the adult mouse retina using adeno-associated viral vectors encoding *Cre* recombinase and short hairpin RNA against *Crb2*. *In vivo* retinal imaging by means of optical coherence tomography on retinas lacking CRB2 in photoreceptors showed progressive thinning of the photoreceptor layer and cellular mislocalization. Electroretinogram recordings under scotopic conditions showed severe attenuation of the a-wave, confirming the degeneration of photoreceptors. Retinas lacking CRB2 in developing photoreceptors showed early onset of abnormal lamination, whereas retinas lacking CRB2 in developing Müller cells showed late onset retinal disorganization. Our data suggest that in the developing retina, CRB2 has redundant functions in Müller glial cells, while CRB2 has essential functions in photoreceptors. Our data suggest that short-term loss of CRB2 in adult mouse photoreceptors, but not in Müller glial cells, causes sporadic loss of adhesion between photoreceptors and Müller cells.

INTRODUCTION

Mutations in the Crumbs homolog-1 (*CRB1*) gene have been reported in patients with a variety of autosomal recessive retinal dystrophies, including Leber congenital amaurosis, retinitis pigmentosa type 12, retinitis pigmentosa with Coats-like exudative vasculopathy and other early-onset forms of retinitis pigmentosa (1–3).

CRB1 is a member of the Crumbs family that in mammals is composed of four members, CRB1, CRB2, CRB3A and CRB3B (3). The prototypic CRB protein has a large extracellular domain with epidermal growth factor (EGF) and

* To whom correspondence should be addressed at: Department of Neuromedical Genetics, The Netherlands Institute for Neuroscience, Meibergdreef 47, 1105 BA, Amsterdam, The Netherlands. Tel: +31 205664597; Fax: +31 205666121; Email: j.wijnholds@nin.knaw.nl

laminin-globular domains, a single transmembrane domain, and a short 37 amino acid intracellular C-terminus containing single FERM and PDZ protein-binding motifs (4). The Crumbs proteins are associated through PALS1 with PATJ or MUPP1, forming the core of the Crumbs complex (5–10). In the developing and adult mouse retina, the apical Crumbs complex resides at the subapical region adjacent to the adherens junctions between the retinal progenitor cells (11) or between the photoreceptors and Müller glial cells (9,12). However, in the adult mouse retina, while CRB2 protein is present in both photoreceptor and Müller glial cells, CRB1 is detected only in Müller glial cells (13).

In the mouse retina, loss of CRB1 from Müller glial cells results in retinal disorganization and dystrophy limited to one quadrant of the retina (9,14). The severity of the *CRB1/Crb1* phenotype is strongly dependent on the genetic background as different mutations cause various retinal phenotypes in human and mice (9,14,15). The lack of a clear genotype–phenotype correlation suggests that other Crumbs family members have a function influencing the severity of the retinal disease. We showed that the removal of CRB2 from retinal progenitor cells resulted in progressive abnormal lamination of newborn photoreceptors leading to severe retinal degeneration with concomitant loss of retinal function (16). Furthermore, CRB2 has roles in restricting proliferation of progenitor cells and the number of rod photoreceptor and Müller glial cells (11,16). Loss of both CRB1 and CRB2, from mouse retinal progenitor cells, results in retinal overgrowth due to overproliferation of retinal progenitor cells, leading to an abnormal and thick retina without a proper and separated photoreceptor cell layer. The Crumbs proteins show a dose-dependent effect, since different levels of CRB protein give rise to different phenotypes (17).

These recent studies helped increase our understanding of the role of CRB2 in the retinal progenitor cells and its influence in retinal development. However, the specific roles of CRB2 in photoreceptor and Müller glial cells, or maintenance of the adult retina structure, remained unclear. Therefore, in this work, we studied the effects of cell-specific loss of CRB2 from the developing mouse retina, using targeted conditional deletion of *Crb2* in photoreceptors or Müller glial cells. We also studied the consequences of targeted loss of CRB2 in adult mouse retinas using adeno-associated viral (AAV) vectors encoding *Cre* recombinase and *short hairpin RNA* (*shRNA*) against *Crb2*.

Our findings show that CRB2 has a redundant function in mouse Müller glial cells; however, in photoreceptor cells, CRB2 is crucial for proper retinal development. Removal of CRB2 from photoreceptors leads to severe and progressive degeneration with a concomitant loss of retinal function. In the adult mouse retina, short-term loss of CRB2 in photoreceptor cells, but not in Müller glial cells, causes sporadic loss of adhesion between adult photoreceptors or Müller glial cells.

RESULTS

Lack of CRB2 during photoreceptor maturation impairs retinal function in adult mice

We studied the specific function of CRB2 in photoreceptor cells, by crossing the *Crb2* floxed homozygous ($Crb2^{F/F}$) mice on a C57BL/6J genetic background (11,16) with Crx-*Cre* (18) to obtain *Crb2*Crx cKO ($Crb2^{F/F}/CrxCre^{+/-}$) animals.

The Crx-*Cre* transgenic mice express CRE recombinase in developing photoreceptors and pinealocytes of the pineal gland. CRE expression was detected at embryonic day (E) 12.5 in postmitotic differentiating photoreceptors (18,19). *Crb2*Crx cKO mice were fertile and in majority viable, but showed a 42% incidence of severe hydrocephalus consistent with the domed head shape. The ventricles of the newborn *Crb2*Crx cKO with hydrocephalus appeared to be drastically dilated, and the subventricular structures were damaged severely (data not shown). Although the cause of hydrocephalus is not clear, hydrocephalus is unlikely to cause or affect the retinal phenotypes we observed.

We performed functional and morphological *in vivo* analysis of the retinal phenotype in 1-, 3- and 5-month(s)-old *Crb2*Crx cKO, and in the respective age-matched control animals, using electroretinography (ERG), scanning laser ophthalmoscopy (SLO) and spectral domain optical coherence tomography (OCT).

By 1 postnatal month, *Crb2*Crx cKO mouse retinas showed a distinct reduction in both scotopic and photopic ERG amplitudes conditions, indicating alterations of both rod and cone system components (Fig. 1A–C). At high stimulus intensities under scotopic conditions, the a-wave of the affected animals was comparatively more reduced than the b-wave. Consequently, the b/a ratio was high, suggesting a primary defect in photoreceptors in *Crb2*Crx cKO mice (Fig. 1C). With increasing age, the ERG signal amplitudes were similar to young animals and no rapid degeneration was observed (Fig. 1D). *In vivo* retinal analysis in 1-month-old *Crb2*Crx cKO mice revealed changes in the fundus appearance as well as in retinal layer morphology, suggesting degenerative processes (Fig. 2F–J). In the bright field illuminated fundus image, several spots and patchy areas were visible, and in the corresponding autofluorescence image, an accumulation of autofluorescent material was seen. In addition, a significant reduction of the thickness of the outer retina was observed, as well as several sites where misplaced cells were detected (Fig. 2I, insets J; Supplementary Material, Fig. S1Q). With increasing age, the *Crb2*Crx cKO mice showed a continued progression of the retinal degeneration, characterized by an increase of the number of fundus abnormalities and a more pronounced thinning of the retina (Fig. 2K–O, P–T and Supplementary Material, Fig. S1R–S). Additionally, in the *Crb2*Crx cKO, the retinal vasculature was abnormal at 1 month of age (Fig. 2H). By fluorescein angiography, sites of neovascularization were observed which were very similar in appearance to vascular abnormalities detected in *Crb2*Chx10 cKO mice (11).

In summary, the data from the *in vivo* analysis indicate that removal of CRB2 from photoreceptor cells (*Crb2*Crx cKO) leads to a severe retinal phenotype with functional impairment.

Removal of CRB2 from photoreceptor cells results in severe and progressive morphological retinal deterioration

In 1-month-old *Crb2*Crx cKO, we found several disruptions of the outer limiting membrane at these sites and observed protrusion of photoreceptors into the subretinal space and misplaced inner retinal cells in the outer plexiform layer (Supplementary Material, Fig. S1B). In the *Crb2*Crx cKO retinas, CRB2 expression was

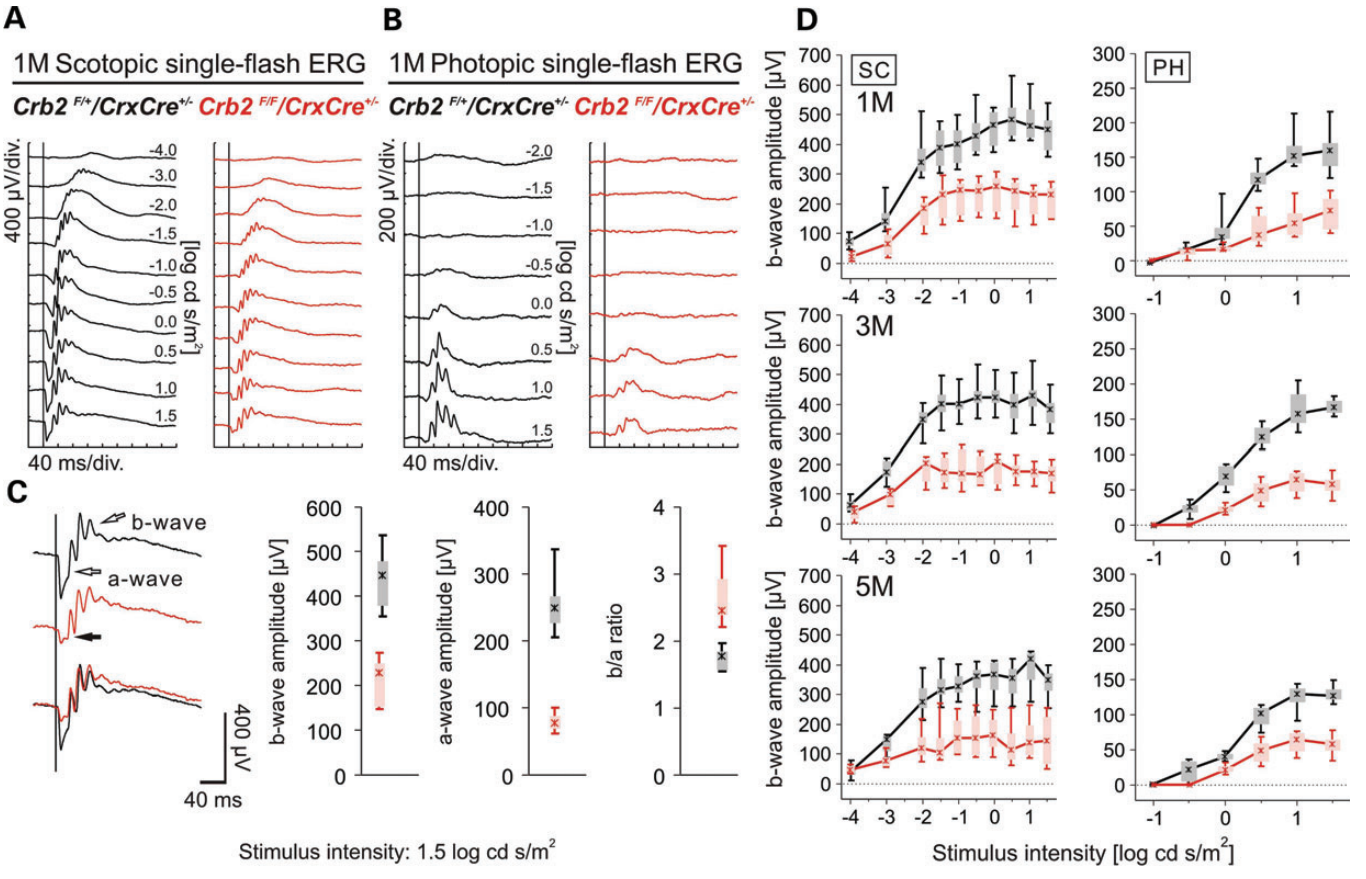

Figure 1. Retinal function is impaired in *Crb2*Crx cKO. Electroretinographic analysis of retinal function in $Crb2^{F/+}/CrxCre^{+/-}$ heterozygous control (black), and $Crb2^{F/F}/CrxCre^{+/-}$ affected mice (*Crb2*Crx cKO, red). (**A**) Scotopic and (**B**) photopic single-flash intensity series from representative animals at the age of 1 month. (**C**) Left: scotopic single-flash ERG responses at 1.5 log cd s/m^2 from a heterozygous and a *Crb2*Crx cKO as well as a respective superposition. The a-wave and the b-wave are indicated by open arrows and the black arrow points to the attenuated a-wave of the *Crb2*Crx cKO (red). Right: Quantitative evaluation of scotopic single-flash b-wave, a-wave amplitudes (1.5 log cd s/m^2) and the corresponding b-wave/a-wave amplitude ratio (b/a ratio). Boxes indicate the 25 and 75% quantile range, whiskers indicate the 5 and 95% quantiles, and the asterisks indicate the median of the data (box-and-whisker plot). (**D**) Time course single-flash ERG data from 1- (top), 3- (middle) and 5- (bottom) month(s)-old mice. Scotopic (SC, left column) and photopic (PH, right column) b-wave amplitude are presented as in (**C**) as a function of the logarithm of the flash intensity (*Vlog*I function) *Crb2*Crx cKO showed a distinct decrease in retinal function. Number of animals used: *Crb2*Crx*Cre*: 1-month-old (1M): four per group; 3M: four *Crb2*Crx cKO and five controls; 5 M: four per group.

lost from the photoreceptor cells (Supplementary Material, Fig. S1H); however, immunohistochemistry indicates a small amount of CRB2 protein was present in Müller glial cells of these retinas (Supplementary Material, Fig. S1H, arrowheads). These retinas displayed a disrupted subapical region and adherens junctions (Supplementary Material, Fig. S1J, L, N and P).

Over time, these retinas continue to progressively thin to the point where, at 3-months of age the outer nuclear layer (ONL) was reduced to 4–6 rows of photoreceptor nuclei, protrusions of photoreceptors into the subretinal space were observed (Supplementary Material, Fig. S1D and R). Sporadically, at 1- and 3-months of age, some residual large photoreceptor rosettes and retinal folds in the ONL were detected (data not shown). At 5-months of age, in some areas, the retinas lacking CRB2 in the photoreceptor cells exhibited regions nearly devoid of photoreceptors, with only a few photoreceptor nuclei remaining (Supplementary Material, Fig. S1F and S).

The adult *Crb2*Crx cKO retinal phenotype most severely affected the photoreceptor cells. We performed immunohistochemistry on 3-month-old retinas using different photoreceptor markers to study in more detail the changes in the photoreceptors. We found recoverin-positive photoreceptor cells in the subretinal space (Fig. 3B, arrowhead). In some areas, the rod photoreceptors (rhodopsin positive) were observed with short or absent outer segments (Fig. 3D, arrowhead), and rhodopsin accumulation was detected in the photoreceptor cell soma (Fig. 3D, arrows, inset). Cone photoreceptors were also affected, in control mice, cone arrestin-positive nuclei were exclusively located at the top of the ONL (Fig. 3E) and displayed well-defined synaptic terminals and outer segments, whereas in the knockout retinas the cones showed absence or significantly shortened outer segments. Some of the nuclei of these cones were displaced to a basal part of the ONL, close to the outer plexiform layer (Fig. 3F). M-opsin-positive cones were similarly affected, and in some areas, we observed mislocalization of M-opsin to the cell soma (Fig. 3H). The phenotype observed in 3-month-old *Crb2*Crx cKO retinas was not limited to the ONL but also affected the inner retina. In the *Crb2*Crx cKO retinas, we observed ectopic SOX9-positive Müller glial cell nuclei in the top of the ONL, at foci of cellular mislocalization (Supplementary Material, Fig. S2B, arrowheads). Disruption of the apical end-feet of these cells could be observed when immunostained with

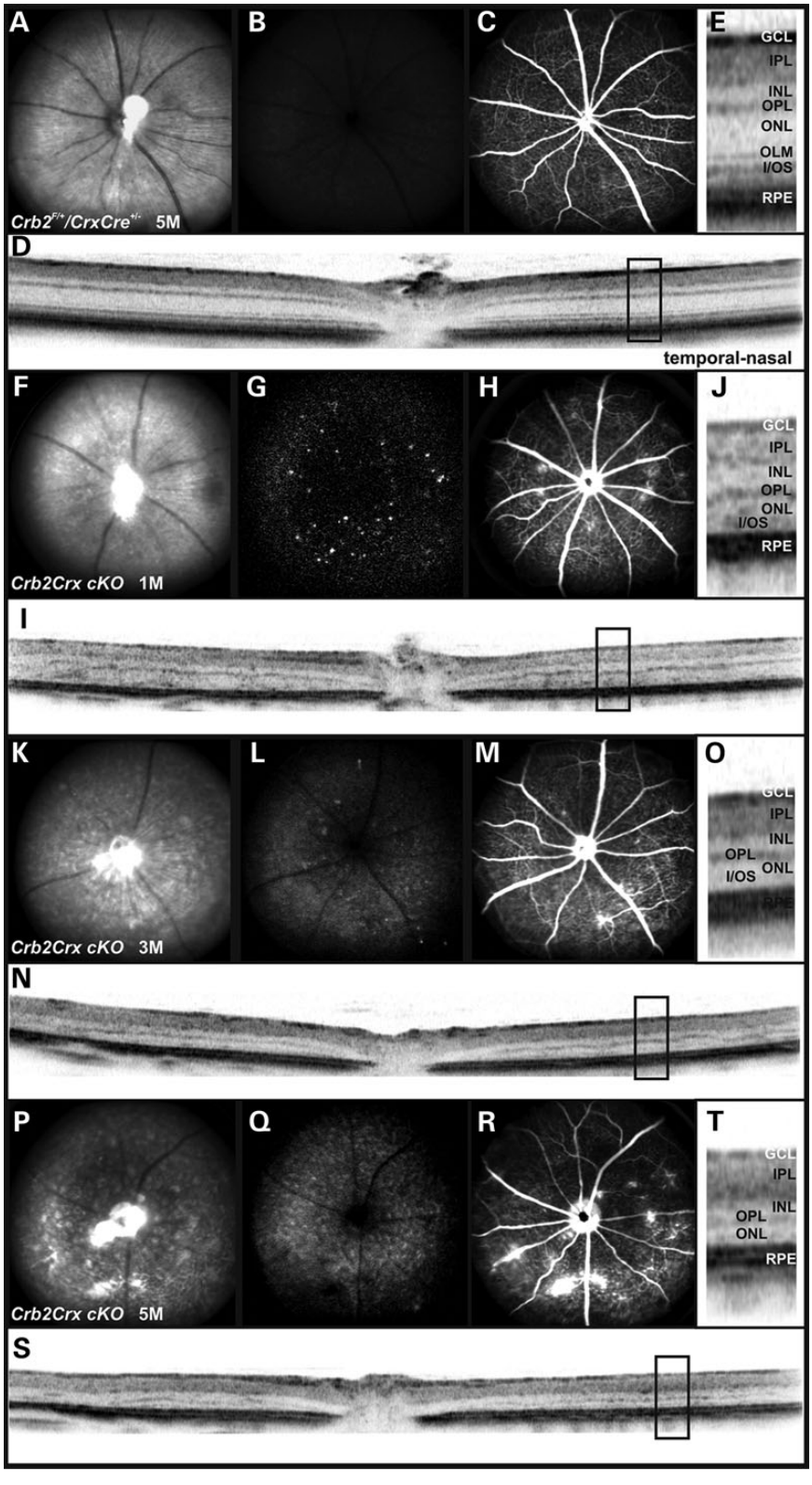

Figure 2. *In vivo* retinal imaging of photoreceptors lacking CRB2 showed progressive degeneration. Retinal morphology in 5-month-old $Crb2^{F/+}/CrxCre^{+/-}$ and in 1-, 3- and 5-month(s)-old *Crb2Crx* cKO mice. Heterozygous and homozygous mice retinas were examined with SLO imaging (**A** and **B** versus **F** and **G** versus **K** and **L** versus **P** and **Q**), fluorescein angiography (**C**, **H**, **M** and **R**) and SD-OCT (**D** and **E**, **I** and **J**, **N** and **O** and **S** and **T**). As a first sign of retinal degeneration, native fundus images at 513 nm revealed a spotty fundus appearance in the affected animals already at the age of 1 month (F) in comparison to the controls (A). Increasing age, the number of spots increased (K and P), as well as the magnitude of hyperfluorescent regions detectable in the autofluorescent images (G, L and Q). With fluorescein angiography, retinal vascular alterations were found all over the fundus at 1 month of age (H) and became more severe at older stages (M and R) in comparison to the controls (C). Horizontal OCT scans across the optic disc revealed a decrease in the retinal thickness already at 1-month of age (I and J) and a thinner retina subsequently at the age of 3 and 5 months (N and O, S and T).

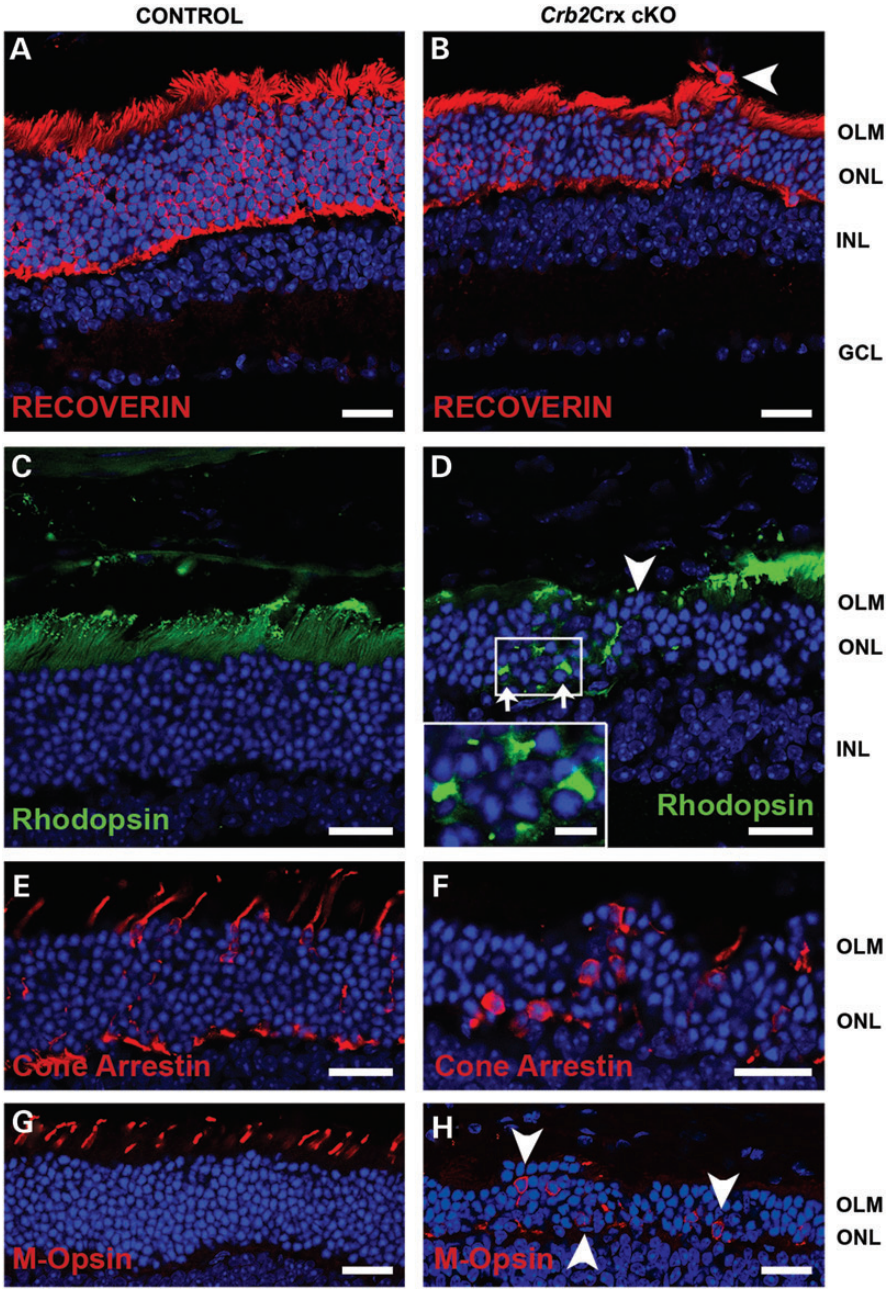

Figure 3. Loss of CRB2 in photoreceptor cells leads to degeneration of the ONL. Immunohistochemistry of 3-month-old *Crb2*Crx-*Cre* mouse retinas. Sections were stained with antibodies against: recoverin (**A** and **B**), rhodopsin (**C** and **D**), cone arrestin (**E** and **F**) and M-opsin (**G** and **H**). In the mutant retinas, the ONL is thinner and disorganized. Several photoreceptor nuclei localized the subretinal space were positive for recoverin (arrowhead) (B). Ectopic rhodopsin expression was found in the cell soma of the photoreceptor in the mutant retinas (arrows, inset) (D). Cone photoreceptors were also affected, in some areas the nuclei of these cells were located in basal position close to the outer plexiform layer (F and H) and the outer segments was shorter or absent (F and H). In these cells, M-opsin localized ectopically in the cell soma (H). No morphological changes were observed in the control retinas. GCL, ganglion cell layer; INL, inner nuclear layer; OLM, outer limiting membrane; ONL, outer nuclear layer. Scale bars: 25 μm, insets in (D): 7.5 μm.

anti-glutamine synthetase (GS) (Supplementary Material, Fig. S2B). The 3-month-old *Crb2*Crx cKO retinas overexpressed glial fibrillary acidic protein (GFAP) throughout the entire retina and the expression was higher at foci of cellular mislocalization (Supplementary Material, Fig. S2D, arrowheads). In *Crb2*Crx cKO retinas, we observed a marked increase of CD11b-positive cells, an immune cell marker (Supplementary Material, Fig. S2F), extended into the outer retinal layers and to misplaced photoreceptors in the subretinal space.

Amacrine (calretinin positive) and ganglion (neuron-specific class III beta-tubulin (Tuj1)-positive) inner retinal neurons were correctly localized at this time point (Supplementary Material, Fig. S2H). Rod bipolar cells, stained with PKCα antibody, were found misplaced in the ONL in areas with photoreceptor

protrusions (Supplementary Material, Fig. S2J and L). The outer plexiform layer was fragmented, as demonstrated by PSD-95 staining and ectopic localization of PSD-95 was also observed in the ONL and close to the misplaced photoreceptor cells in the subretinal space suggesting the presence of ectopic photoreceptor synapses (Supplementary Material, Fig. S2J and L).

CRB2 in photoreceptors is required for proper retinal development and lamination

The severe phenotype observed in the adult *Crb2*Crx cKO retinas suggests that CRB2 in photoreceptors has an important role in retinal development. To study this in additional detail, we analyzed retinas at embryonic (E12.5, E15.5 and E18.5) and early postnatal (P3, P6 and P10) time points. The first morphological abnormalities were detected at E15.5; at this time, rosettes were occasionally found in the neuroepithelial layer at the periphery of the retina (Fig. 4B, arrowhead). At E18.5, disruptions of the outer limiting membrane were observed at the periphery (Fig. 4D, arrowhead) and occasional photoreceptor rosettes in the neuroepithelial layer. Misplaced inner retinal cells were found in the neuroepithelial layer and adjacent to the retinal pigment epithelium (Fig. 4D, arrows). Using immunohistochemistry, we demonstrated that the expression of CRB2 was largely reduced in E18.5 *Crb2*Crx cKO retinas but some remaining CRB2 protein was still detected in the knockout retinas, most likely due to CRB2 present in adjacent wild-type radial glial progenitors and early Müller glial cells (Fig. 4L, arrowheads). Disruptions of the subapical region stained by anti-MUPP1 (Fig. 4N), and of the adherens junctions stained by anti-β-catenin and anti-Nectin1 (Fig. 4P and R), were observed. At these areas, mislocalized nuclei were present close to the retinal pigment epithelium. Rosettes expressing in their center adherens junction markers such as β-catenin were also found (Fig. 4P).

At postnatal Day 3, we found two types of rosettes in the periphery of the retina, the first composed of photoreceptor cells in the middle of the neuroepithelial layer (Fig. 4F, arrowhead) and the second composed of inner retina cells at the top of the neuroepithelial layer (Fig. 4F, arrow). Disruptions of the outer limiting membrane were observed. Transmission electron microscopy pictures of *Crb2*Crx cKO retinas showed the presence of misplaced photoreceptor nuclei in the subretinal space adjacent to the retinal pigment epithelium (Fig. 5B and C). In some regions, these nuclei were located between the inner segments of the photoreceptors and the retinal pigment epithelium (Fig. 5B, asterisks). Adherens junctions were present in the knockout retinas; however, their distribution and localization was irregular (Fig. 5B, arrowheads). The microvilli from the retinal epithelium cells were compressed between the ectopic photoreceptor nuclei and the apical membrane of the retinal pigment epithelium (Fig. 5B and C, arrows).

At postnatal Day 6, we observed similar abnormalities as at postnatal Day 3, with the addition of single or small clusters of ectopic photoreceptor nuclei in the subretinal space and small disruptions of the outer limiting membrane throughout the entire retina (Fig. 4H, arrowheads).

Retinas from 10-day-old *Crb2*Crx cKO mice showed a very prominent phenotype, throughout the entire retina, with disruptions of the outer limiting membrane that coincided with protrusions of photoreceptor cells into the subretinal space (Fig. 4J). At this time point, a huge accumulation of photoreceptor nuclei in the subretinal space was observed, forming a double layer of photoreceptors (Fig. 6D). Rosettes and retinal folds were also frequently observed (Fig. 6B, D, F, H and J). In the center of these (half-)rosettes, we found fragments of outer limiting membrane positive for subapical region (PALS1) and adherens junction (N-cadherin) markers (Fig. 6B). As observed at postnatal Days 3 and 6, two types of rosettes could be found, one mainly composed of photoreceptor cells (Fig. 6D) and another composed of inner retinal cells such as amacrine (PAX6- and/or calretinin positive) (Fig. 6F, arrowhead, insets), rod bipolar cells (PKCα positive) (Fig. 6H, arrowheads) and Tuj1-positive ganglion cells (Fig. 6J, arrow). The interneuron-containing rosettes were found near the bottom of the ONL or trapped between different photoreceptor rosettes, these cells seemed to project processes into the center of the rosettes. We also detected ectopic localization of the synaptic marker PSD-95 around the photoreceptor rosettes (Fig. 6H).

The lamination of Müller glial cell nuclei was affected. We detected SOX9-positive nuclei around the photoreceptor cell rosettes (Fig. 6J). Although the lamination of these retinas was severely affected, we did not detect an increase in GFAP expression at this time point (data not shown).

In P10 *Crb2*Crx cKO retinas, ectopic nuclei were detected in the ganglion cell layer (Fig. 6D, arrowhead and F, arrow). Some of these nuclei were recoverin positive and might therefore be photoreceptors or cone bipolar cells (Fig. 6D, arrowheads).

Removal of CRB2 from Müller glial cells results in a mild retinal phenotype

To delete *Crb2* in Müller glial cells, we crossed $Crb2^{F/F}$ with Pdgfrα-*Cre* (20) transgenic mouse lines, to obtain *Crb2*Pdgfrα cKO ($Crb2^{F/F}/Pdgfr\alpha Cre^{+/-}$) animals. In this transgenic mouse line, CRE expression is directed to nearly all retinal Müller glial cells by the mouse Pdgfrα (platelet-derived growth factor receptor, alpha polypeptide) promoter. However, some CRE expression may also be observed in the ONL and in the ganglion cell layer (20). *Crb2*Pdgfrα cKO were viable and fertile; however, they were born at a 5-fold reduced ratio than expected. The *Crb2*Pdgfrα cKO group examined at 5 postnatal months showed no functional or morphological differences when analyzed by ERG, SLO or OCT (Fig. 7).

In *Crb2*Pdgfrα cKO retinas, we observed at 1-, 3- and 5-month(s) of age disruptions of the outer limiting membrane, where rows of photoreceptor nuclei protruded into the subretinal space. These disruptions were mainly observed at the periphery of the retina (Fig. 8B, D and F). The gross morphology of the retina remained preserved, confirming the *in vivo* data. However, at 5M, a significant reduction of the ONL thickness was found compared with control retinas (Fig. 8F′). Although CRB2 was removed from Müller glial cells, the protein was still present in the photoreceptor cells, resulting only in a slight reduction in the signal of CRB2 staining (Fig. 8H). At foci, we observed small disruptions in the staining of Crumbs complex members such as CRB1 (Fig. 8J), PALS1 (Fig. 8L), MUPP1 (Fig. 8N), the PAR complex member PAR3 (Fig. 8P), adherens junction markers β-catenin (Fig. 8R), catenin pp120 (P120) (Fig. 8T), Nectin1 (Fig. 8V), zonula occludens-1 (ZO-1) (Fig. 8X) and N-cadherin (Fig. 8Z). Protrusion of photoreceptor

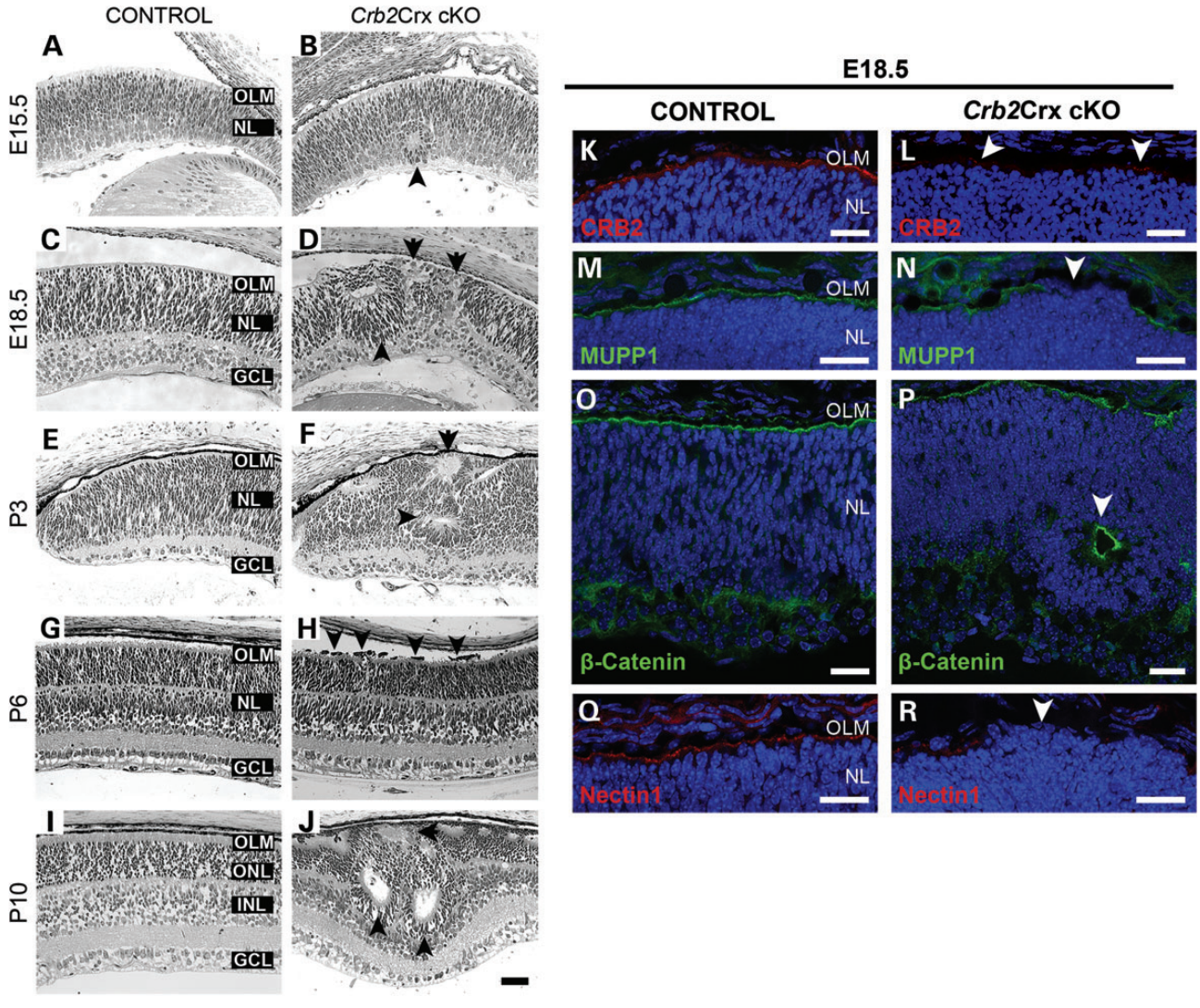

Figure 4. Loss of CRB2 from photoreceptor cells results in retinal disorganization. Toluidine-stained light microscope pictures of retinal sections, from the control (**A**, **C**, **E**, **G** and **I**) and from the *Crb2*Crx cKO (**B**, **D**, **F**, **H** and **J**), at different ages, (A and B)—E15.5, (C and D)—E18.5, (E and F)—P3, (G and H)—P6 and (I and J)—P10. No abnormalities were observed in the control. At E15.5, we observed the first morphological alterations in the mutant retinas with sporadic rosettes in the neuroepithelial layer at the periphery of the retina (arrowhead) (B). At E18.5, the phenotype became more obvious with disruptions of the outer limiting membrane and rosettes formation at the periphery (arrowhead) (D), in the proximity of rosettes misplaced inner retinal cells localized adjacent to the retinal pigmented epithelium (arrows) (D). At P3, disruptions of the outer limiting membrane and photoreceptor cell rosettes were found in the periphery of the retina (arrowhead) (F). Another type of rosette of cells that morphologically resemble inner retinal cells localized at the top of the outer limiting membrane just adjacent to the retinal pigment epithelium (arrow) (F). At P6, we observed similar abnormalities as at P3; however, at this time point, we also detected single or small clusters of ectopic photoreceptor nuclei in the subretinal space throughout the entire retina (arrowheads) (H). At P10, disruptions of the outer limiting membrane coincided with protrusions of photoreceptor cells into the subretinal space. Rosettes and retinal folds were also frequently observed (J). Immunohistochemistry pictures from control (**K**, **M**, **O** and **Q**) and *Crb2*Crx cKO (**L, N, P** and **R**) retinal sections stained for apical markers at E18.5: CRB2 (K and L), MUPP1 (M and N), β-catenin (O and P) and Nectin1 (Q and R). CRB2 was mostly absent from the subapical region in the knockout retinas; however, some CRB2 was still detectable (arrowheads), much likely due to CRB2 expression in adjacent wild-type progenitor and Müller glial cells (L). In the knockout retinas, the outer limiting membrane was disrupted at foci, with loss of MUPP1 (N), β-catenin (P) and nectin1 (R). Sporadically, rosettes were observed at E18.5 (arrowhead) (P). GCL, ganglion cell layer; INL, inner nuclear layer; NL, neuroepithelial layer; OLM, outer limiting membrane; ONL, outer nuclear layer; RPE, retinal pigment epithelium; SAR, subapical region. Scale bars: (A–H): 50 μm; (I–P): 25 μm.

nuclei into the subretinal space at sites of outer limiting membrane disruption were observed in the mutant retinas (Fig. 8H, J and T). Five-month-old *Crb2*Pdgfrα cKO retinas showed a very mild phenotype; however, we observed ectopic Müller glial cell nuclei in the ONL (Fig. 9B, arrowheads) and activated Müller glial cells, characterized by a moderate increase in the expression of GFAP, mainly at foci of cellular mislocalization (Fig. 9D, arrowheads). At these places, ectopic expression of CD11b, a marker for immune cells, was detected (Fig. 9F).

In summary, removal of CRB2 from Müller glial cells results in a mild anatomical phenotype with no detectable effects on retinal function measured by ERG.

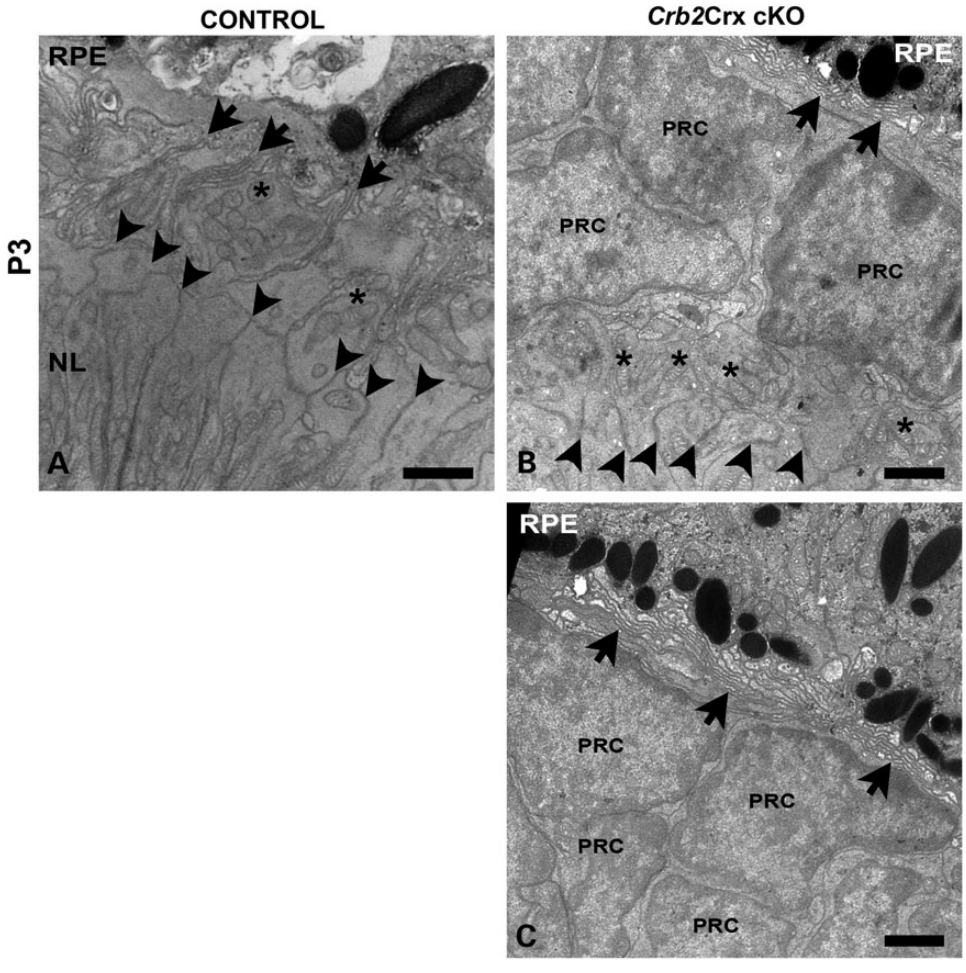

Figure 5. Ultra-structure of retinas lacking CRB2 in photoreceptor cells. Transmission electron microscopy pictures of retina sections, from control (**A**) and *Crb2*Crx cKO (**B** and **C**) retinas, at postnatal Day 3. In the control retinas, the adherens junctions were well aligned and showed a regular distribution (A, arrowheads), and proper arrangement of photoreceptor inner segments was observed (A, asterisks). Properly ordered microvilli from the retinal pigment epithelium span from the apical membrane until the photoreceptor inner segments (A, arrows). In *Crb2*Crx cKO retinas, we observed misplaced photoreceptor nuclei in the subretinal space adjacent to the retinal pigment epithelium (B and C). In some regions, these nuclei were located between the inner segments of the photoreceptors and the retinal pigment epithelium (B, asterisks). Adherens junctions were present in the knockout retinas; however, their distribution and localization was irregular (B, arrowheads). The microvilli of the retinal pigment epithelium cells were compressed between the ectopic photoreceptor nuclei and the apical membrane of the retinal pigment epithelium (B and C, arrows). Photoreceptor nuclei (asterisk). Scale bar: 1 μm. NL, neuroepithelial layer; PRC, photoreceptor cells; RPE, retinal pigment epithelium.

Decreased levels of CRB2 in adult photoreceptor cells induces mild disorganization of the retina

To study the cell-specific function of CRB2 in the adult retina, different AAV vector approaches were used for cell-specific transduction. We used AAV-mediated CRE gene transfer (21) into *Crb2* floxed retinal cells (11,16) to knockout *Crb2* expression. Otherwise, we used AAV-mediated short hairpin *Crb2* transfer into wild-type C57BL/6J retinal cells to silence *Crb2* expression.

For photoreceptor-specific transduction via the subretinal route, an AAV2-based vector was packaged in AAV5 capsid (AAV2/5) (22). The AAV-*Cre* vectors were tested for potential toxicity by delivery of different numbers of genome copies (10^8, 10^9, 10^{10}) of AAV into wild-type retinas. Three weeks after injection, the retinas were examined for morphological abnormalities. No toxicity and/or retinal damage was observed due to *Cre* expression (data not shown). Based on these results, to target photoreceptors we applied 10^9 AAV2/5 cytomegalovirus promoter (CMV)-*CRE-GFP* or 10^{10} AAV2/5 human G-protein-coupled receptor kinase 1 (GRK1) promoter-*CRE-GFP* genome copies (1 μl) by subretinal injection into $Crb2^{F/F}$ retinas.

Subretinal delivery of AAV2/5 CMV-*CRE-GFP*, that expresses a CRE-GFP fusion protein, led to nuclear expression of CRE in photoreceptors and in retinal pigment epithelial cells. $Crb2^{F/F}$ retinas infected with AAV2/5 CMV-*CRE-GFP* showed decreased immunostaining for CRB2 and gaps in the staining in areas containing GFP-CRE-positive photoreceptor nuclei (Fig. 10B, B′). We observed sporadically rows of ectopic photoreceptor nuclei protruding into the subretinal space (0–1 event per representative retinal section), some of these displaced nuclei were GFP-CRE-positive while others were negative (Fig. 10D, arrowhead), suggesting lack of adhesion between these cells. *Cre* transduced retinas presented disruptions of the outer plexiform layer, stained by PSD-95 and ectopic localization of this protein in the ONL (data not shown).

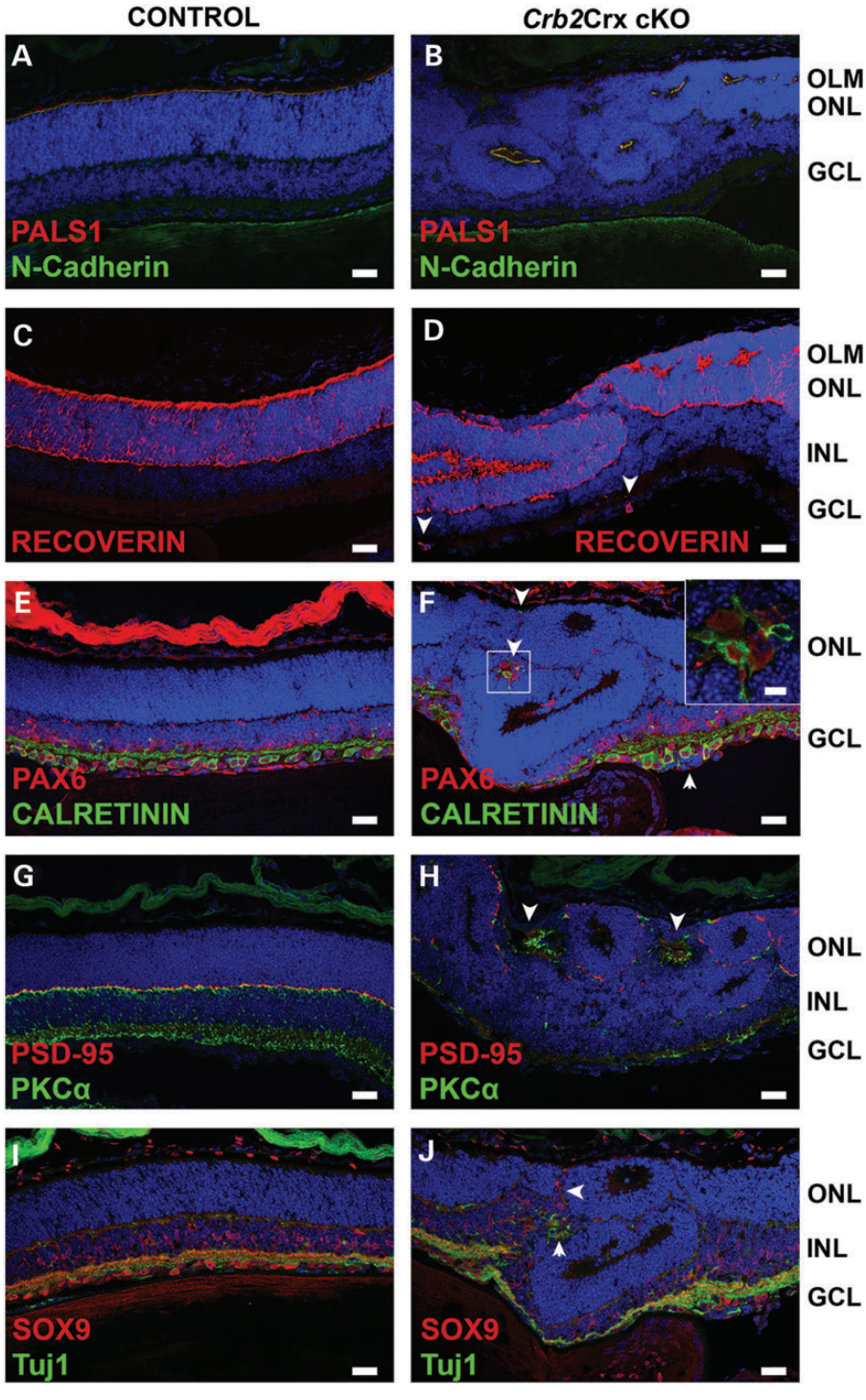

Figure 6. Lack of CRB2 in photoreceptor cells affects retinal lamination. Immunohistochemistry of 10-day-old *Crb2*Crx-*Cre* mouse retinas. Sections were stained with antibodies against: PALS1 and N-cadherin (**A** and **B**), recoverin (**C** and **D**), PAX6 and (c) alretinin (**E** and **F**), PSD-95 and PKCα (**G** and **H**), SOX9 and neuron-specific class III beta-tubulin (Tuj1) (**I** and **J**). At P10 in the mutant retinas, disruptions at the outer limiting membrane and ectopic photoreceptor nuclei in the subretinal space were detected. In some areas, multiple (half-)rosettes or retinal folds were detected. In the center of the rosettes, apical proteins, such as PALS1 and N-cadherin (B), were observed. Adjacent to these (half-)rosettes, several cell types were misplaced. Recoverin (a marker for photoreceptor and cone bipolar cells)-positive cells were found in the ganglion layer (arrowheads) (D). Also interneurons, amacrine cells (PAX6 and/or calretinin positive) (F, arrowheads) and PKCα-positive bipolar cells (H, arrowheads) were found misplaced in the middle or on the top of the ONL in areas where rosettes were found. Ectopic localization of PSD-95 was found around the rosettes (H). In some areas, PAX6 and calretinin negative cells in the ganglion cell layer were detected (F, arrow). Also, misplaced Müller glial cell nuclei (SOX9 positive) (J, arrowhead) and ganglion cells (Tuj1 positive) (J, arrow) were found. No morphological changes were observed in the control retinas. GCL, ganglion cell layer; INL, inner nuclear layer; OLM, outer limiting membrane; ONL, outer nuclear layer. Scale bars: 25 μm, insets in (D): 7.5 μm.

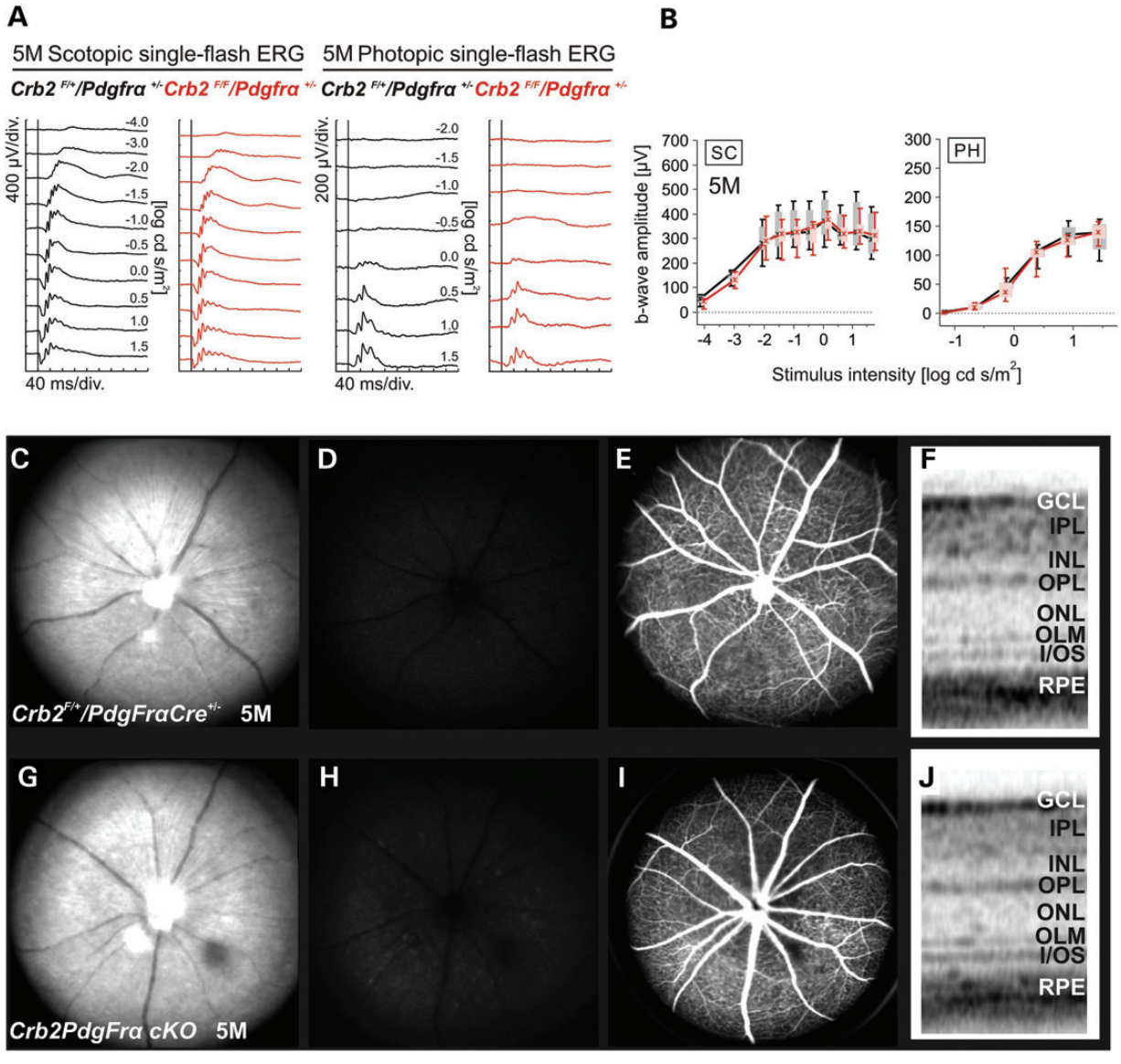

Figure 7. Loss of CRB2 in Müller glial cells did not result in functional alterations. (**A**) Electroretinogram data from 5-month-old $Crb2^{F/+}/Pdgfr\alpha Cre^{+/-}$ heterozygous control (black), and $Crb2^{F/F}/Pdgfr\alpha Cre^{+/-}$ mice (*Crb2Pdgfr*α cKO, red). (**B**) Quantification of the scotopic and photopic b-wave amplitude of control and cKO mice shown as box-and-whisker plot. The *Crb2*Pdgfrα cKO did not show alteration in retinal function. Number of animals used: four *Crb2*Pdgfrα cKO and five controls. Retinal morphology in 5-month-old *Crb2Pdgfrα* cKO mice and age-matched controls. *Crb2Pdgfrα* control and cKO mice were examined with SLO imaging (**C** and **D** versus **G** and **H**), fluorescein angiography (**E** and **I**) and SD-OCT (**F** and **J**). Native fundus imaging at 513 nm revealed a regular fundus appearance in the affected animals (**G**) in comparison to control (C), no fluorescent material was detected in the autofluorescence image (H). Horizontal OCT scans revealed a regular retinal layering in the affected (J) and in the control mice (F). GC, ganglion cell layer; IPL, inner plexiform layer; INL, inner nuclear layer; OPL, outer plexiform layer; ONL, outer nuclear layer; OLM, outer limiting membrane; I/OS, inner/outer segment; RPE, retinal pigment epithelium.

To prevent expression in the retinal pigment epithelium, we used a photoreceptor-specific promoter, human GRK1 in AAV2/5 GRK1-*CRE-GFP* for expression of CRE-GFP specifically in photoreceptors (23). Subretinal administration of the AAV2/5 GRK1-driven constructs restricted the expression of GFP and CRE-GFP to the photoreceptor cells, no GFP-positive retinal pigment epithelial or inner retinal cells were detected (Fig. 10E and F). We observed a decrease in the signal of CRB2 staining in areas transduced by the AAV2/5 GRK1-*CRE-GFP* (Fig. 10F, F′) in contrast to non-transduced areas (data not shown). The gross structure of the retina was preserved, but we detected sporadically small morphological abnormalities similar as described for the AAV2/5 CMV-*CRE-GFP* vector, such as disruptions of the outer plexiform layer stained by MPP4, and ectopic localization of this protein in the ONL (data not shown).

A complementary strategy to silence the expression of *Crb2* using shRNA was designed. We selected two shRNA constructs, targeting exon 2 and exon 9a, that revealed a silencing efficiency of ∼70% of a GFP-tagged *Crb2* expression vector (data not shown). The pSUPER-based sh*Crb2* constructs, including the polymerase-III H1-RNA gene promoter (H1), were subcloned

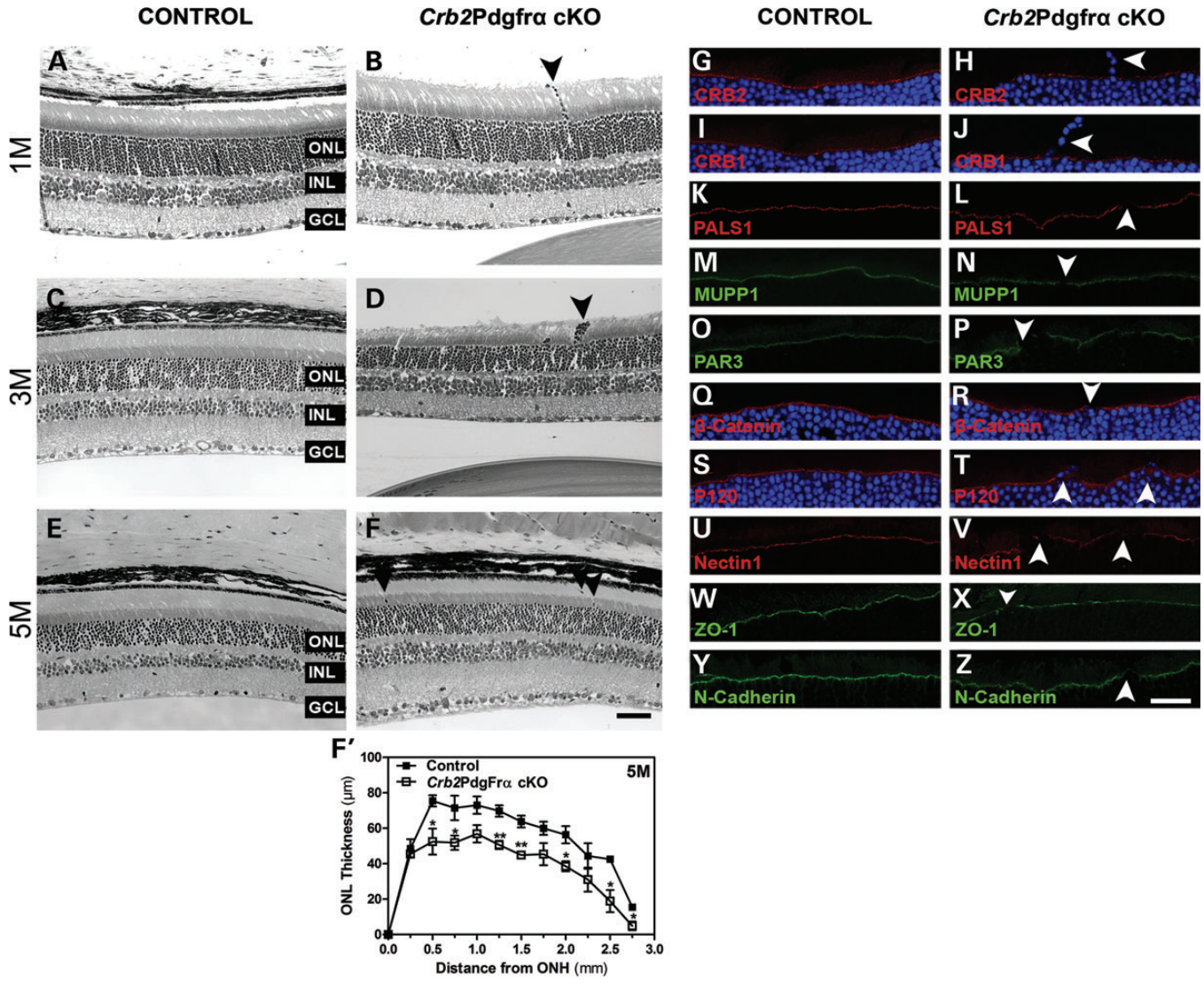

Figure 8. Loss of CRB2 from Müller glial cells results in mild retinal disorganization. Toluidine-stained light microscopy of retinal sections from control (**A**, **C** and **E**) and *Crb2*Pdgfrα cKO (**B**, **D** and **F**), at different ages, (A and B) – 1M, (C and D) – 3M, (E and F) – 5M. No abnormalities were observed in the control. At 1, 3 and 5 month(s), gaps were detected in the outer limiting membrane and single photoreceptor nuclei or rows nuclei were observed in the subretinal space (B, D and F). Quantification of the ONL thickness (F′) plotted from the distance to the ONH showed a significant thinning in $n = 3$ *Crb2*Pdgfrα cKO retinas at 5 months compared with $n = 3$ control retinas. Most of the morphological alterations observed in the mutant retinas were limited to the periphery of the retina. Immunohistochemistry of 5-month-old *Crb2*Pdgfrα-*Cre* retinal sections were stained for subapical region markers: CRB2 (**G** and **H**), CRB1 (**I** and **J**), PALS1 (**K** and **L**), MUPP1 (**M** and **N**), PAR3 (**O** and **P**) and for adherens junction markers: β-catenin (**Q** and **R**), catenin pp120 (P120) (**S** and **T**), Nectin1 (**U** and **V**), ZO-1 (**W** and **X**), N-cadherin (**Y** and **Z**). CRB2 protein was still detectable due to CRB2 expression in wild-type photoreceptor cells in the knockout retina (H). CRB1, PALS1 and MUPP1 staining showed disruption of the CRB complex at the subapical region at sites of cellular mislocalization, in the periphery of the retina (J, L and N). PAR3 was also lost at sites of disruption (P). Staining using adherens junctions markers: β-catenin (R), P120 (T), Nectin1 (V), ZO-1 (X) and N-cadherin (Z) showed disruption of the adherens junctions mainly in the periphery. Moreover, ectopic photoreceptor nuclei protruded into the subretinal space (H and J). No morphological changes were observed in the control retinas. GCL, ganglion cell layer; INL, inner nuclear layer; OLM, outer limiting membrane; ONH, optic nerve head; ONL, outer nuclear layer; RPE, retinal pigment epithelium. Scale bars: (A–F) 50 μm; (G–Z) 25 μm. Data are presented as mean ± SEM; $n = 3$–4. $^{*}P < 0.05$; $^{**}P < 0.01$.

into an AAV2-vector containing a CMV-*GFP* expression marker (CMV-*GFP*-H1-sh*Crb2*). The two sh*Crb2* constructs gave similar results.

As a control, we used a CMV-*GFP*-H1-sh*Mpp4* described before (13). MPP4 is present in the photoreceptor synapses and at lower levels at the subapical regions of photoreceptor cells (6). Retinas from *Mpp4* knockout mice only sporadically showed photoreceptor displacement, without changing the CRB protein complex at the outer limiting membrane, adherens junctions or the structure of the photoreceptor synapse (24) but caused disruption of photoreceptor synaptic MPP4 protein complexes (25,26).

Subretinal delivery of AAV2/5 coding shRNA (CMV-*GFP*-H1-shRNA), in wild-type retinas (C57BL/6J), drove GFP expression in the cytoplasm of photoreceptor cells and retinal pigment epithelium. Occasionally, some GFP-positive cells were found in the inner nuclear layer (Fig. 11A). Retinas from animals injected with the AAV2/5 CMV-*GFP*-H1-sh*Mpp4* control

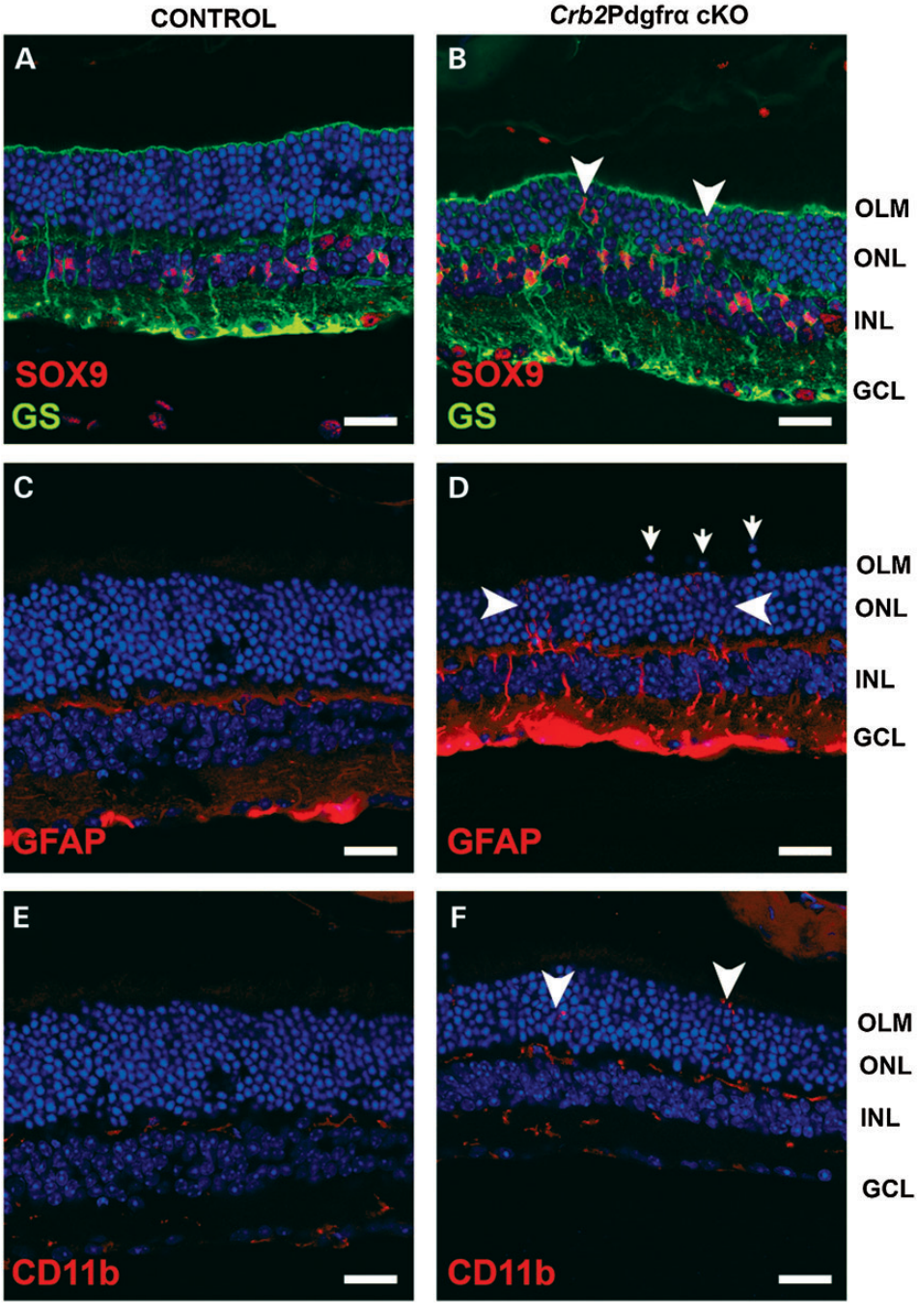

Figure 9. Removal of CRB2 from Müller glial cells results in mild gliosis. Immunohistochemistry of 5-month-old *Crb2*Pdgfrα-*Cre* mouse retinas. Sections were stained with antibodies against: SOX9 and GS (**A** and **B**), GFAP (**C** and **D**), CD11b (**E** and **F**). In the mutant retinas, several Müller glial nuclei were misplaced in the ONL (B, arrowheads), also some photoreceptor nuclei were misplaced in the subretinal space (D, arrows). The mutant retinas showed activated Müller glia cells, detected by an increase in the GFAP staining (D, arrowheads). An increase in immune cell marker in the ONL, stained by anti-CD11b, was detected (F). No morphological changes were observed in the control retinas. GCL, ganglion cell layer; INL, inner nuclear layer; OLM, outer limiting membrane; ONL, outer nuclear layer. Scale bars: 25 μm.

vector (10^9 genome copies, 1 μl) showed no observable abnormalities in retinal architecture (Fig. 11A). In sh*Mpp4* injected retinas, no differences in the levels of CRB2 immunoreactivity between transduced and non-transduced areas were found (Fig. 11C, C′ and data not shown).

sh*Crb2* transduced retinas did show sporadic protrusions (0–1 event per representative retinal section) of GFP-positive photoreceptor cell nuclei in the subretinal space (Fig. 11B, arrowhead and F, arrow). Immunostaining with anti-CRB2 showed reduced immunoreactivity in areas transduced with the AAV2/5

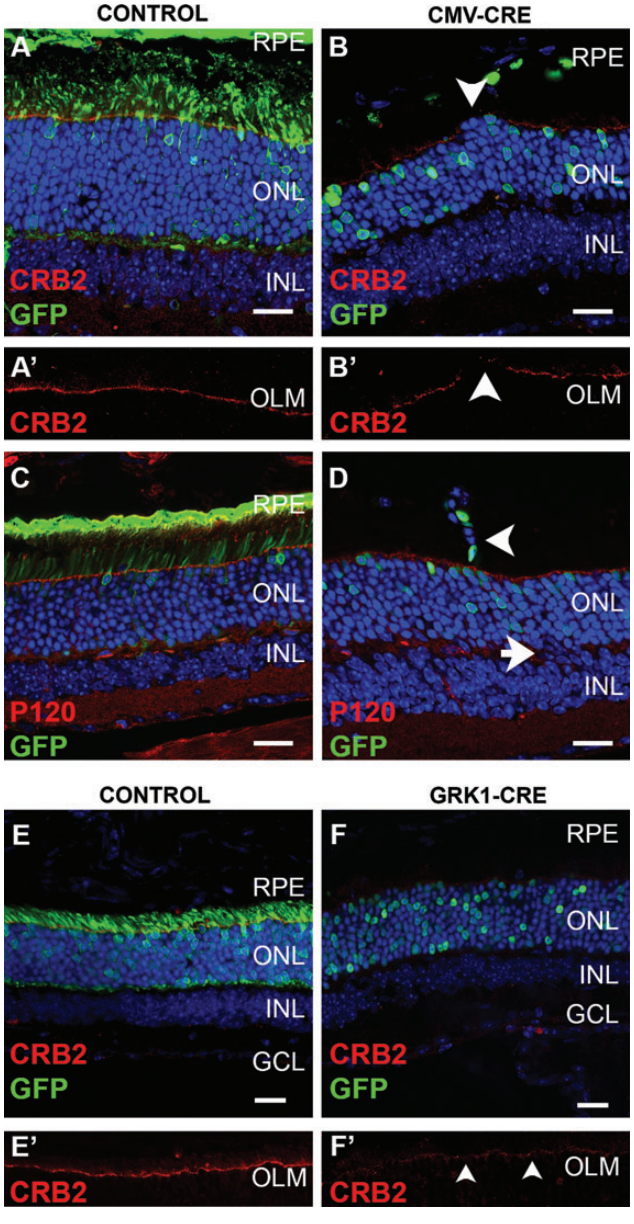

Figure 10. Photoreceptor-specific knockout of *Crb2* using *Cre* viral vectors. Immunohistochemistry of 7-week-old $Crb2^{F/F}$ retinas infected at 4 weeks-of-age with AAV2/5 CMV-*GFP* (control) (**A**, **A′**, **C**), AAV2/5 CMV-*CRE-GFP* (**B**, **B′**, **D**), AAV2/5 GRK1-*GFP* (control) (**E**, **E′**) or AAV2/5 GRK1-*CRE-GFP* (**F**, **F′**). AAV2/5 CMV-*CRE-GFP* vectors expressed GFP or CRE-GFP in photoreceptor cells and retinal pigmented epithelium (**A**, **C** and **B**, **D**). AAV2/5 GRK1-*CRE-GFP* vectors expressed GFP or CRE-GFP specifically in photoreceptor cells (E and F). Sporadically, disruptions of anti-CRB2 staining in subapical regions were found (B and B′). Misplaced CRE-positive and CRE-negative photoreceptor cells were detected in the subretinal space (D, arrowhead). In some areas, the outer plexiform layer was thinner and the outer and inner nuclear layers contacted each other (D, arrow). GCL, ganglion cell layer; INL, inner nuclear layer; OLM, outer limiting membrane; ONL, outer nuclear layer; RPE, retinal pigment epithelium. Scale bars: 20 μm.

CMV-*GFP*-H1-sh*Crb2* (Fig. 11D, D′, arrowheads). Reduction of the CRB2 signal correlated with the increase in GFP signal, indicating that decrease in CRB2 occurred specifically in the transduced photoreceptors (Fig. 11D′). Immunostaining with

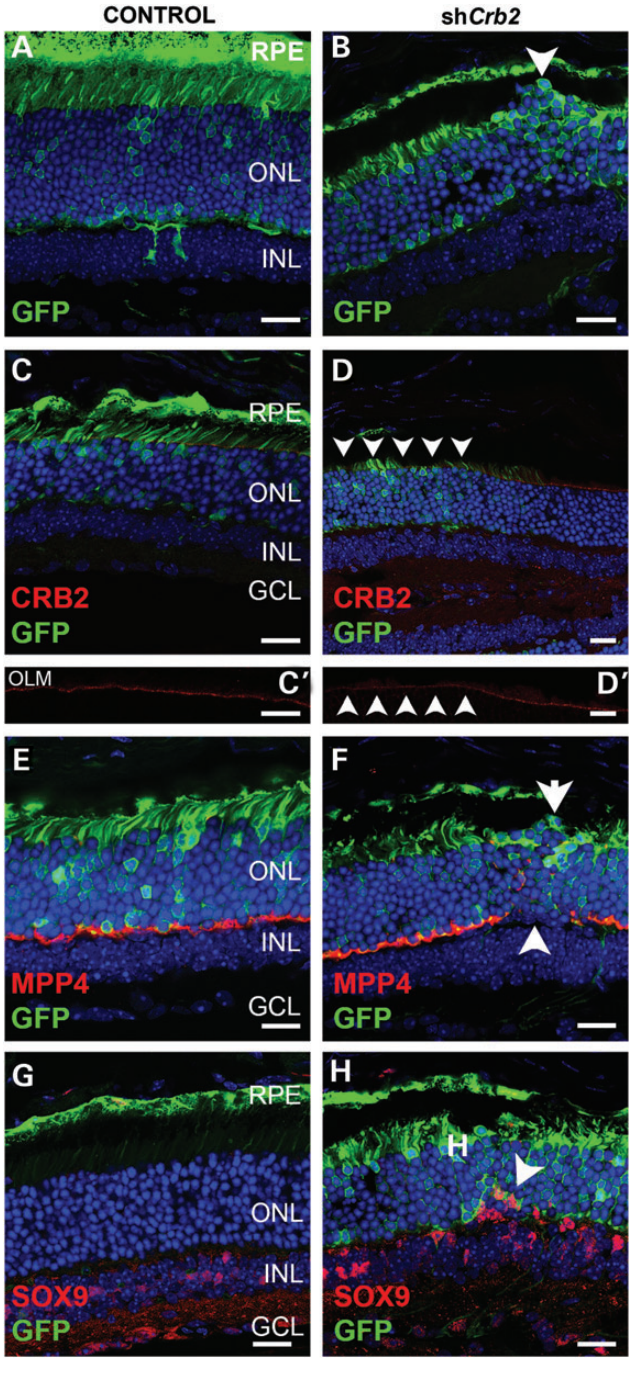

Figure 11. Photoreceptor-specific knockdown of *Crb2* using AAV2/5 CMV-*GFP*-H1-*shRNA*. Immunohistochemistry of 7-week-old wild-type (C57BL/6J) retinas infected at 4 weeks-of-age with AAV2/5 CMV-*GFP*-H1-sh*Mpp4* (control) or AAV2/5 CMV-*GFP*-H1-sh*Crb2*. AAV2/5 CMV-*GFP*-H1-sh*RNA* drives *GFP* and sh*RNA* expression in the retinal pigment epithelium (RPE) and in the photoreceptor cells (**A**–**H**). Expression of the control sh*Mpp4*, in photoreceptors and RPE did not lead to morphological abnormalities (A, C, E and G). Expression of sh*Crb2* leads to decrease of CRB2 protein at foci, which colocalized with increased number of GFP-positive cells (D and **D′**). At foci, we observed misplaced GFP-positive photoreceptor nuclei in the subretinal space (B, F and H) and disruption of the outer plexiform layer with ectopic localization of MPP4 (F, arrowhead). Ectopic Müller glia cell SOX9-positive nuclei were also detected (H, arrowhead). GCL, ganglion cell layer; INL, inner nuclear layer; OLM, outer limiting membrane; ONL, outer nuclear layer; RPE, retinal pigment epithelium. Scale bars: 20 μm.

anti-MPP4 showed a slight immunoreactivity reduction at the outer plexiform layer in transduced areas (Fig. 11E). sh*Crb2* transduced areas showed foci of disruptions of the outer plexiform layer stained with MPP4 (Fig. 11F). Ectopic MPP4 in the ONL was detected, suggesting mislocalized photoreceptor synapses (Fig. 11F, arrowhead). Misplaced Müller glial SOX9-positive nuclei in the ONL were also found in sh*Crb2* transduced areas (Fig. 11H, arrowhead).

Decreased levels of CRB2 in adult Müller glial cells do not affect the retina integrity

For Müller glial cell-specific transduction via the intravitreal route, an AAV2-based vector was packaged in ShH10Y445F capsid (AAV2/ShH10Y) (27,28), 10^{10} genome copies of AAV2/ShH10Y CMV-*CRE-GFP* (1 μl) by intravitreal injection into floxed $Crb2^{F/F}$ retinas. Previously, others showed high selectivity of the AAV2/ShH10Y vector for rat Müller glial cells when administered in the retina by the intravitreal route (27). Here, we demonstrated that, 3 weeks after intravitreal injection of 10^{10} genome copies, AAV2/ShH10Y CMV-*GFP* (Supplementary Material, Fig. S3A) drove GFP expression in the cytoplasm of mouse Müller glial cells, identified by their characteristic morphology, with their nuclei located in the inner nuclear layer and processes spanning across the entire retina. GFP expression colocalized with Müller glial cell markers such as GS and SOX9 (data not shown). Expression of AAV2/ShH10Y CMV-*CRE-GFP* resulted in nuclear expression of CRE-GFP in Müller glial cells (Supplementary Material, Fig. S3B). CRE expression in $Crb2^{F/F}$ adult Müller glial cells did not result in a detectable reduction of CRB2 immunoreactivity at the subapical region (Supplementary Material, Fig. S3B, B′), likely due to expression of CRB2 in adjacent photoreceptors. No disruptions in the subapical region and/or in the adherens junctions were observed when stained with anti-CRB2 and anti-catenin-pp120 (Supplementary Material, Fig. S3B). The levels of GFAP expression were similar in CMV-*GFP* and CMV-*CRE-GFP* injected retinas (data not shown), suggesting that intravitreal injection and subsequent *CRE-GFP* expression in adult Müller glial cells did not induce additional retinal stress.

AAV2/ShH10Y CMV-*GFP*-H1-sh*Crb2* viral particles (10^9 genome copies) were injected intravitreously to silence the expression of *Crb2* in wild-type C57BL/6J Müller glial cells. These experiments gave similar results (Supplementary Material, Fig. S3D) as described before for the AAV2/ShH10Y CMV-*CRE-GFP* conditional knockout viral vector. These results are in line with the data obtained from the *Crb2*Pdgfrα cKO mice reinforcing the hypothesis that CRB2 has redundant roles in Müller glial cells.

DISCUSSION

In this study, we demonstrated that (i) in the developing retina, CRB2 has a redundant function in Müller glial cells. (ii) CRB2 is essential in photoreceptors for proper retinal lamination and function. (iii) In the adult retina, short-term loss of CRB2 in photoreceptor cells, but not in Müller glial cells, causes sporadic loss of adhesion between adult photoreceptors or Müller glial cells. Moreover, we developed new tools that allowed us to drive *CRE* expression specifically in Müller glial cells (AAV2/ShH10Y CMV-*CRE-GFP*) or in photoreceptor cells (AAV2/5 GRK1-*CRE-GFP*), to perform *Crb2* silencing *in vivo* (AAV2/shH10Y CMV-*GFP*-H1-sh*Crb2* and AAV2/5 CMV-*GFP*-H1-sh*Crb2*).

In the developing mouse retina, CRB2 was detected in retinal progenitor cells and in the adult retina in photoreceptors and Müller glial cells (11,13). In *Crb2*Crx cKO retinas, removal of CRB2 in photoreceptor precursor cells results in a severe phenotype, with an early onset (E15.5). Crx-*Cre* expression starts at E12.5 with a prominent expression at E15.5 (18). This suggests efficient CRE-mediated recombination that results in loss of CRB2 expression, photoreceptor adhesion and polarity. We previously showed that loss of CRB2 through Chx10-*Cre*-mediated recombination resulted in a morphological phenotype at E18.5 (11), later than observed in the *Crb2*Crx cKO (E15.5). The Chx10-*Cre* transgenic mouse line showed high degree of mosaicism (29), suggesting that *Crb2*Chx10 cKO retinas were composed of a mixture of wild-type and mutant cells, that may be sufficient to retain normal morphology until later embryonic stages (11). The onset and levels of expression and recombination efficiency in the Crx-*Cre* and Chx10-*Cre* mice could also differ, giving rise to this difference.

Loss of CRB2 from photoreceptors results in lamination defects that affect mainly rod and cone photoreceptors, suggesting a lack of adhesion between these cells giving rise to giant retinal folds and rosettes. However, in contrast with the observation made in the *Crb2*Chx10 cKO (11,13), in the *Crb2*Crx cKO the lamination of ganglion, amacrine, bipolar and Müller glial cells was also affected, misplaced inner retinal cells were detected ectopically in the ONL. Similar defects in the lamination of these cells were also observed in CRB2 null retinas with half of the amount of CRB1 ($Crb1^{+/-}$ *Crb2*Chx10 cKO) (17). These results are in line with (i) previous zebrafish data where Crb2a is required for retinal cell patterning and lamination (30) and (ii) mouse data where the CRB-interacting protein PALS1 affected the correct patterning of photoreceptor cells (31,32).

Müller glial cells are one of the latest cell types to be born in the retina. They are generated between E15 and P10, the majority of Müller cells are born around postnatal Day 5 (33). Lack of CRB2 in Müller cells resulted in a mild phenotype mainly affecting the periphery of the retina, with a slow progression and without detectable functional consequences for the entire retina. Mouse retinas lacking CRB1 in Müller glial cells showed loss of maintenance of adhesion between photoreceptors and Müller glial cells as observed in the *Crb2*Pdgfrα cKO; however, in CRB1 null retinas, the lesions were restricted to the inferior temporal quadrant of the mouse eye (34), whereas in *Crb2*Pdgfrα cKO retinas the lesions are detected throughout the retina. We hypothesize that CRB1 in Müller glial cells (14,34) compensated in *Crb2*Pdgfrα cKO retinas for the loss of CRB2. We recently demonstrated that removal of CRB1 in a CRB2 null retina exacerbate the CRB2 phenotype in a dose-dependent manner (17). Thus, mouse retinas with complete depletion of CRB1 and CRB2 from Müller glial cells could answer this question.

Recently, we reported that removal of CRB2, from progenitor cells, resulted in loss of other apical and adherens junction protein markers, suggesting that reduction in CRB2 levels leads to destabilization of the whole CRB complex and its

interacting complexes (11,16). Here, we demonstrated that removal of CRB2 from either Müller glial or photoreceptors has similar effect on the apical complexes. This is partially in consonance with observations in PALS1 mutant mice (31,32), and consistent with the epithelial polarity and adhesion defects seen in both the *Drosophila Crb* mutant and the zebrafish *Crb2a* (*ome*) mutant (12,35,36).

Short-term depletion of CRB2 in the adult retinas demonstrated that CRB2 is required for maintenance of the retinal structure. Moreover, CRB2 in early photoreceptors is essential for proper retinal lamination and function.

Intravitreally administered AAV2/ShH10Y vector infects up to 53% of all Müller glial cells in the rat retina (27) and shows similar transduction characteristics in mice (L.P.P. and J.W., unpublished results). By immunohistochemistry, we did not detect significantly reduced levels of CRB2 at the subapical region in CRB2-depleted Müller glial cells. In part, this could be due to relatively high levels of CRB2 in photoreceptors. In addition, in *Crb2*Pdgfrα cKO retinas, we did not detect a drastic decrease of CRB2 at the subapical region adjacent to adherens junctions between Müller glial cells and photoreceptors. The lack of severe morphological phenotype can be explained in part by compensation by CRB1 in Müller glial cells. Further *Crb2* gene silencing studies in *Crb1* null background retinas could provide further information. Our preliminary unpublished data suggest that silencing *Crb2* in adult *Crb1* null mouse retinas did not result in an exacerbation of the retinal phenotype.

In humans, mutations in *CRB1* are responsible for 10–15% of Leber congenital amaurosis cases and for ∼4% of all cases of retinitis pigmentosa (1–3,37–39). So far, no mutations in *CRB2* have been associated with retinal degeneration. However, it cannot be excluded that some sequence variants may contribute to retinal disease (40). Conditional deletion of *Crb2*, specifically in early progenitors, results in disorganization during late retinal development leading to severe and progressive retinal degeneration with concomitant retinal function loss that mimics retinitis pigmentosa due to mutations in the *CRB1* gene (11). Here, we showed that the presence of CRB2 in photoreceptor cells is crucial for proper retinal development, removal of CRB2 from these cells, resulted in severe progressive degeneration with a concomitant loss of retinal function. These data open new perspectives about the clinical approach in the development of *CRB1* gene therapy treatment for Leber's congenital amaurosis and retinitis pigmentosa.

MATERIALS AND METHODS

Animals

All procedures concerning animals were performed with permission of the animal experimentation committee (DEC) of the Royal Netherlands Academy of Arts and Sciences (KNAW), permit numbers NIN 06-46, 12-106, 11-54 and 12-59. All mice used were maintained on a 99.9% C57BL/6J genetic background. Animals were maintained on a 12 h day–night cycle and supplied with food and water *ad libitum*. Mice did not have *rd8* or *pde6b* mutations.

Crb2 conditional knockout mice (11,16) were crossed with Crx-*Cre* (Tg(Crx-cre)1Tfur) (18) or with a Pdgfrα-*Cre* (C57BL/6-Tg(Pdgfrα-cre)1Clc/J) (20) transgenic mouse lines, obtained from Dr Furukawa or the Jackson Laboratory, respectively, to remove *Crb2* from the photoreceptor and from Müller glial cells, respectively. The analysis of *Crb2*Crx-*Cre* mice was performed using only male animals, whereas analysis of *Crb2*Pdgfrα-*Cre* was on females and males.

Chromosomal DNA isolation and genotyping

Ear biopsies were incubated in lysis buffer (50 mM Tris, pH 8.0, 100 mM NaCl, 1% SDS) with Proteinase K (0.5 mg/ml) at 55°C for 16 h. The isopropanol precipitated chromosomal DNA was washed with 80% ethanol and rehydrated in TE buffer. Genotyping of the *Crb2* floxed transgenic animals were performed as previously described (11). The following primers were used to detect the transgenic *Cre* expression: *RV60* 5′-GACGATGCAA CGAGTGATGA-3′, *RV61* 5′-AGCATTGCTGTCACTTGGTC-3′ (product size 300 bp). The gender of *Crb2*Crx-*Cre* embryos and early postnatal animals was performed as described before (41): forward primer: 5′-CTGAAGCTTTTGGCTTTGAG-3′, reverse primer: 5′-CCACTGCCAAATTCTTTGG-3′ targeting two homologs X- and Y-linked genes (*Jarid1c* and *Jarid1d*) that differ in intron sizes resulting in a single 302 bp (female) or double (302 and 331 bp) (male) PCR product.

In vivo analysis

ERG, spectral domain optical coherence tomography (SD-OCT) and SLO measurements were performed in the same session. Animals from the two mouse lines: *Crb2*Crx-*Cre* of 1-, 3-, 5-month(s)-old and *Crb2*Pdgfrα-*Cre* of 5-month-old were analyzed. The different age groups were composed of 4–5 animals of each genotype: controls ($Crb2^{F/+}/Cre^{+/-}$) and *Crb2* cKO ($Crb2^{F/F}/Cre^{+/-}$). Electroretinograms were performed according to previously described procedures (42). The ERG equipment consisted of a Ganzfeld bowl, a direct current amplifier and a PC-based control and recording unit (Multiliner Vision). Animals were dark-adapted overnight and anesthetized with ketamine (66.7 mg/kg body weight) and xylazine (11.7 mg/kg body weight). Pupils were dilated with tropicamide eye drops (Mydriaticum Stulln, Pharma Stulln, Stulln, Germany). Single-flash responses were obtained under dark-adapted (scotopic) and light-adapted (photopic) conditions. Light adaptation was accomplished with a background illumination of 30 cd/m^2 starting 10 min before photopic recordings. Single white-flash stimuli ranged from −4 to 1.5 log cd s/m^2 under scotopic and from −2 to 1.5 log cd s/m^2 under photopic conditions. Ten responses were averaged with interstimulus intervals of 5 s (for −4 to −0.5 log cd s/m^2) or 17 s (for 0–1.5 log cd s/m^2).

SD-OCT imaging was performed with a commercially available Spectralis^{TM} HRA+OCT device from Heidelberg Engineering featuring a broadband superluminescent diode at $\lambda =$ 870 nm as low coherent light source (42). Each two-dimensional B-Scan recorded with the equipment set to 30° field of view, consists of 1536 A-scans acquired at a speed of 40 000 scans per second. Optical depth resolution is ∼7 μm with digital resolution reaching 3.5 μm. Imaging was performed using the proprietary software package Eye Explorer (version 3.2.1.0, Heidelberg Engineering).

Retinal structures of the anesthetized animals were visualized via SLO imaging with an HRA 1 and HRA 2 (Heidelberg Engineering, Heidelberg, Germany) according to previously described procedures (43). Briefly, HRA 1 and HRA 2 systems feature two lasers (488/514 nm) in the short (visible) wavelength range and two (795/830 nm and 785/815 nm) in the long (infrared) wavelength range. The 488 and 795 nm lasers are used for fluorescein and indocyanine green angiography, respectively.

Morphological and immunohistochemical analysis

Eyes were collected at different time points: *Crb2*Crx-*Cre*, embryonic day (E) 12.5, 15.5, E18.5, postnatal day (P) 3, P6, P10, 1-month-old (1M), 3M, 5M mice ($n = 4–6$/age group); *Crb2*Pdgfrα-*Cre*, 1M, 3M and 5M mice ($n = 4–6$/age group). For morphological analysis, eyes were enucleated and fixed at room temperature with 4% paraformaldehyde in PBS for 20 min. After fixation, the eyes were dehydrated for 30 min in 30, 50, 70, 90 and 96% ethanol and embedded in Technovit 7100 (Kulzer, Wehrheim, Germany), according to the manufacture instructions and sectioned (3 μm). Slides were dried, counterstained with 0.5% toluidine blue and mounted under coverslips using Entellan (Merk, Darmstadt, Germany). The thickness of the ONL in 1-month-old (1M), 3M, 5M *Crb2*Crx-*Cre* and 5M *Crb2*Pdgfrα-*Cre* mice and control ($n = 3–4$/age group) was measured on the Technovit sections every 250 μm from the optic nerve head (ONH). The two measurements apart from the optic nerve head were averaged, plotted and compared with control retinas. For immunohistochemical analysis, eyes from the animals were enucleated and fixed during 20 min in 4% paraformaldehyde in PBS. Subsequently, the tissues were cryo-protected with 30% sucrose in PBS, embedded in Tissue-Tek O.C.T Compound (Sakura, Finetek) and used for cryosectioning. Cryosections (7 μm) were rehydrated in PBS. Samples were blocked for 1 h using 10% goat serum, 0.4% Triton X-100 and 1% bovine serum albumin (BSA) in PBS. The primary antibodies (Supplementary Material, Table S1) were diluted in 0.3% goat or donkey serum, 0.4% Triton X-100 and 1% BSA in PBS and incubated for 16 h at 4°C. Fluorescent-labeled secondary antibodies were goat anti-mouse or goat anti-rabbit IgGs conjugated to Cy3 or Alexa 488 (1:500; Jackson Immunoresearch, Stanford, CA, USA and Life Technologies) were diluted in 0.1% goat serum in PBS and incubated for 1 h at room temperature. Nuclei were counterstained with DAPI and mounted in Vectashield hardset mounting medium (H1500, Vector Laboratories, Burlingame, CA, USA). Sections were imaged on a Leica SP5 CLSM. Confocal images were processed with Adobe Photoshop CS6 extended v13.0 ×64.

GENERATION AND PURIFICATION OF THE VIRAL VECTORS

AAV GFP and CRE-GFP vectors

The AAV vector pTRCGW (5.6 kb) containing *GFP* and *CRE-EGFP* (a kind gift from Joost Verhaagen, The Netherlands Institute for Neuroscience, Amsterdam, The Netherlands), carrying the ampicillin resistance gene, inverted terminal repeats (ITR), human immediate early CMV, woodchuck posttranscriptional regulatory element (WPRE) and multiple restriction sites, was used to construct the rAAV*Cre* vector plasmid, as described in (21). To specific targeting of photoreceptor cells, the CMV promoter in the original plasmid was replaced by a 299 bp human GRK1 promoter fragment (23), using the *Spe*I and *Xho*I restriction sites. AAV stocks were generated and purified as described previously (44). Briefly, plasmids containing the transgene flanked by the ITRs were co-transfected with the AAV5 pDP5RS packaging plasmid (Plasmid Factory, Bielefeld, Germany) or AAV-ShH10Y445F packaging plus pHelper plasmids (27) into HEK293 T cells to generate cross-packaged AAV2/5 and AAV2/ShH10Y445F viral vectors (45,46). At the third day after transfection, the medium was changed for lysis buffer (50 mM Tris, 2 mM $MgCl_2$, 150 mM NaCl and 0.1% Triton X-100). After DNAse treatment, the crude lysate was loaded onto an iodixanol density gradient (Sigma, St. Louis, MO, USA) and centrifuged for 70 min in a Beckman XL-100K ultracentrifuge at 69 000 rpm at 16°C (47). Fractions containing the viral vectors were collected and concentrated using Amicon Ultra-15 concentrators. All viral titers were determined by q-PCR and all viral stocks with titers $>1 \times 10^{12}$ genome copies/ml were stored at −80°C until use.

AAV H1-shRNA vectors

For Crb2 silencing by shRNA, five different DNA constructs, against different exons of the *Crb2* gene, were generated by annealing DNA oligonucleotides. The primers were purchased from Eurogentec (Seraing, Belgium). Annealed primers were cloned into the *Hin*dIII and *Bgl*II sites of the pSUPER vector (48). The empty pSUPER and pSUPER-*GFP* shRNA vectors were used as a control. pSUPER-*Crb2* shRNA constructs were co-transfected in HEK293T cells with GFP-tagged Crb2 and subcloned into *Hin*dIII/*Bgl*II of pEGFP-C1 (Clontech), in order to test the knockdown efficiency. Five days after transient transfection, cells were lysed and protein was evaluated by immunoblot analysis with anti-GFP. The experiments were performed in triplicate and three independent experiments were performed. The two shRNA constructs targeting exon 2 and exon 9a, which showed the highest knockdown efficiency *in vitro* were selected for *in vivo* studies and subcloned into the AAV2-CMV-*GFP* vector as described before: (E2-*shCrb2*) 5′-gatccccGTGCCAGGCTACAGAAAGTttcaagagaACTTTCTGTAGCCTGGCACttttggaaa-3′ and (E9a-*shCrb2*) 5′-gatccccTGACTTCTACTGCACCTGCttcaagagaGCAGGTGCAGTAGAAGTCAttttggaaa-3′. The pSUPER-Crb2 *shRNA* vectors were digested with *Xba*I−*Kpn*I and blunted. The selected *shCrb2* fragments including the polymerase-III H1-RNA gene promoter were blunt ligated into an AAV2-CMV-*GFP* vector, which was digested with *Sph*I (two sites after the WPRE and polyA) and blunted. The AAV2-CMV-*GFP*-H1-*shMpp4* was used as a control (13). AAV2/5 and AAV2/ShH10Y445F (27) viral vectors coding E2-*shCrb2*, E9a-*shCrb2* and *shMpp4* were generated.

Intravitreal and subretinal injections

Three- to 4-week-old mice were anesthetized with 100 mg/kg ketamine and 5 mg/kg xylazine by intraperitoneal injection. The pupils were dilated with eye drops that contain 5 mg/ml

tropicamide (Chauvin Benelux, Brussels, Belgium). To prevent dehydration of the cornea, the eyes were treated with viscotears (Novartis Pharma, Arnhem, the Netherlands). The mice were placed on a heating pad to maintain their body temperature at 37°C during the whole procedure. Subsequently, $1 \times 10^{9-10}$ genome copies of vector in 1 μl were either subretinally or intravitreally injected using a 33 gauge needle (Hamilton, Bonaduz, Switzerland). Three to four eyes per viral vector were used. The mice were allowed to recover and their eyes were treated with 10 mg/g chloramphenicol (Ratiopharm, Zaandam, the Netherlands) to prevent infections. Eyes were collected 3 weeks after injection.

The potential toxicity of the AAV2/5 and AAV2/ShH10Y CMV-*CRE-GFP* and of the AAV2/5 GRK1-*CRE-GFP* was tested in 1-month-old wild-type C57BL/6J mice, by delivery of different numbers of genome copies (10^8, 10^9 and 10^{10}, four eyes per condition were injected). Injected retinas examined 3 weeks after injection.

Statistical analysis

Normality of the distribution was tested by Kolmogorov–Smirnov test. Statistical significance was calculated by using *t*-test of 3–4 independent retinas/genotype/age. Values were expressed as mean ± SEM. Values of $^{*}P < 0.05$, $^{**}P < 0.01$ and $^{***}P < 0.001$ were considered to be statistically significant. Statistics and graphs were generated using GraphPad Prism 5.

SUPPLEMENTARY MATERIAL

Supplementary Material is available at *HMG* online.

ACKNOWLEDGEMENTS

We thank Penny Rashbass for providing the pEGFP-C1 *Crb2* construct and the CRB2 antibody (SK11). We thank Alicia Sanz and Iswariyaraja Gurubaran for generating and testing the pSUPER-*Crb2* shRNA constructs. We thank Rein Hoogstraaten, Moniek Nieuwendijk, Gudrun Utz and Pia Lacroix for technical assistance. The authors thank J.J. Dudok for advice on the manuscript.

Conflict of Interest statement. None declared.

FUNDING

This work was supported by Rotterdamse Vereniging Blindenbelangen, Landelijke St. voor Blinden en Slechtzienden, St. Blindenhulp, St. Oogfonds Nederland, St. Retina Nederland, Netherlands Institute for Neuroscience (J.W.), Foundation Fighting Blindness (TA-GT-0811-0540-NIN to J.W. and TA-GT-0313-0607-NIN to J.G.F. and J.W.) and The Netherlands Organisation for Health Research and Development (ZonMw grant 43200004 to J.W.), European Union (HEALTH-F2-2008-200234 to M.W.S. and J.W.).

REFERENCES

1. den Hollander, A.I., ten Brink, J.B., de Kok, Y.J., van Soest, S., van den Born, L.I., van Driel, M.A., van de Pol, D.J., Payne, A.M., Bhattacharya, S.S., Kellner, U. *et al.* (1999) Mutations in a human homologue of Drosophila crumbs cause retinitis pigmentosa (RP12). *Nat. Genet.*, **23**, 217–221.
2. den Hollander, A.I., Davis, J., van der Velde-Visser, S.D., Zonneveld, M.N., Pierrottet, C.O., Koenekoop, R.K., Kellner, U., van den Born, L.I., Heckenlively, J.R., Hoyng, C.B. *et al.* (2004) CRB1 mutation spectrum in inherited retinal dystrophies. *Hum. Mutat.*, **24**, 355–369.
3. Richard, M., Roepman, R., Aartsen, W.M., van Rossum, A.G., den Hollander, A.I., Knust, E., Wijnholds, J. and Cremers, F.P. (2006) Towards understanding CRUMBS function in retinal dystrophies. *Hum. Mol. Genet.*, **15**, R235–R243.
4. Tepass, U., Theres, C. and Knust, E. (1990) crumbs encodes an EGF-like protein expressed on apical membranes of Drosophila epithelial cells and required for organization of epithelia. *Cell*, **61**, 787–799.
5. Bulgakova, N.A. and Knust, E. (2009) The Crumbs complex: from epithelial-cell polarity to retinal degeneration. *J. Cell Sci.*, **122**, 2587–2596.
6. Kantardzhieva, A., Gosens, I., Alexeeva, S., Punte, I.M., Versteeg, I., Krieger, E., Neefjes-Mol, C.A., den Hollander, A.I., Letteboer, S.J., Klooster, J. *et al.* (2005) MPP5 recruits MPP4 to the CRB1 complex in photoreceptors. *Invest. Ophthalmol. Vis. Sci.*, **46**, 2192–2201.
7. Kantardzhieva, A., Alexeeva, S., Versteeg, I. and Wijnholds, J. (2006) MPP3 is recruited to the MPP5 protein scaffold at the retinal outer limiting membrane. *FEBS J.*, **273**, 1152–1165.
8. Assemat, E., Bazellieres, E., Pallesi-Pocachard, E., Le Bivic, A. and Massey-Harroche, D. (2008) Polarity complex proteins. *Biochim. Biophys. Acta*, **1778**, 614–630.
9. van de Pavert, S.A., Kantardzhieva, A., Malysheva, A., Meuleman, J., Versteeg, I., Levelt, C., Klooster, J., Geiger, S., Seeliger, M.W., Rashbass, P. *et al.* (2004) Crumbs homologue 1 is required for maintenance of photoreceptor cell polarization and adhesion during light exposure. *J. Cell Sci.*, **117**, 4169–4177.
10. Roh, M.H., Makarova, O., Liu, C.J., Shin, K., Lee, S., Laurinec, S., Goyal, M., Wiggins, R. and Margolis, B. (2002) The Maguk protein, Pals1, functions as an adapter, linking mammalian homologues of Crumbs and Discs Lost. *J. Cell Biol.*, **157**, 161–172.
11. Alves, C.H., Sanz Sanz, A., Park, B., Pellissier, L.P., Tanimoto, N., Beck, S.C., Huber, G., Murtaza, M., Richard, F., Sridevi Gurubaran, I. *et al.* (2013) Loss of CRB2 in the mouse retina mimics human retinitis pigmentosa due to mutations in the CRB1 gene. *Hum. Mol. Genet.*, **22**, 35–50.
12. Pellikka, M., Tanentzapf, G., Pinto, M., Smith, C., McGlade, C.J., Ready, D.F. and Tepass, U. (2002) Crumbs, the Drosophila homologue of human CRB1/RP12, is essential for photoreceptor morphogenesis. *Nature*, **416**, 143–149.
13. van Rossum, A.G., Aartsen, W.M., Meuleman, J., Klooster, J., Malysheva, A., Versteeg, I., Arsanto, J.P., Le Bivic, A. and Wijnholds, J. (2006) Pals1/Mpp5 is required for correct localization of Crb1 at the subapical region in polarized Muller glia cells. *Hum. Mol. Genet.*, **15**, 2659–2672.
14. Mehalow, A.K., Kameya, S., Smith, R.S., Hawes, N.L., Denegre, J.M., Young, J.A., Bechtold, L., Haider, N.B., Tepass, U., Heckenlively, J.R. *et al.* (2003) CRB1 is essential for external limiting membrane integrity and photoreceptor morphogenesis in the mammalian retina. *Hum. Mol. Genet.*, **12**, 2179–2189.
15. Bujakowska, K., Audo, I., Mohand-Said, S., Lancelot, M.E., Antonio, A., Germain, A., Leveillard, T., Letexier, M., Saraiva, J.P., Lonjou, C. *et al.* (2012) CRB1 mutations in inherited retinal dystrophies. *Hum. Mutat.*, **33**, 306–315.
16. Alves, C.H., Bossers, K., Vos, R.M., Essing, A.H., Swagemakers, S., van der Spek, P.J., Verhaagen, J. and Wijnholds, J. (2013) Microarray and Morphological Analysis of Early Postnatal CRB2 Mutant Retinas on a Pure C57BL/6J Genetic Background. *PLoS ONE*, **8**, e82532.
17. Pellissier, L.P., Alves, C.H., Quinn, P.M., Vos, R.M., Tanimoto, N., Lundvig, D.M., Dudok, J.J., Hooibrink, B., Richard, F., Beck, S.C. *et al.* (2013) Targeted ablation of crb1 and crb2 in retinal progenitor cells mimics leber congenital amaurosis. *PLoS Genet.*, **9**, e1003976.
18. Nishida, A., Furukawa, A., Koike, C., Tano, Y., Aizawa, S., Matsuo, I. and Furukawa, T. (2003) Otx2 homeobox gene controls retinal photoreceptor cell fate and pineal gland development. *Nat. Neurosci.*, **6**, 1255–1263.
19. Koike, C., Nishida, A., Akimoto, K., Nakaya, M.A., Noda, T., Ohno, S. and Furukawa, T. (2005) Function of atypical protein kinase C lambda in

differentiating photoreceptors is required for proper lamination of mouse retina. *J. Neurosci.*, **25**, 10290–10298.
20. Roesch, K., Jadhav, A.P., Trimarchi, J.M., Stadler, M.B., Roska, B., Sun, B.B. and Cepko, C.L. (2008) The transcriptome of retinal Muller glial cells. *J. Comp. Neurol.*, **509**, 225–238.
21. Ahmed, B.Y., Chakravarthy, S., Eggers, R., Hermens, W.T., Zhang, J.Y., Niclou, S.P., Levelt, C., Sablitzky, F., Anderson, P.N., Lieberman, A.R. *et al.* (2004) Efficient delivery of Cre-recombinase to neurons in vivo and stable transduction of neurons using adeno-associated and lentiviral vectors. *BMC Neurosci.*, **5**, 4.
22. Yang, G.S., Schmidt, M., Yan, Z., Lindbloom, J.D., Harding, T.C., Donahue, B.A., Engelhardt, J.F., Kotin, R. and Davidson, B.L. (2002) Virus-mediated transduction of murine retina with adeno-associated virus: effects of viral capsid and genome size. *J. Virol.*, **76**, 7651–7660.
23. Khani, S.C., Pawlyk, B.S., Bulgakov, O.V., Kasperek, E., Young, J.E., Adamian, M., Sun, X., Smith, A.J., Ali, R.R. and Li, T. (2007) AAV-mediated expression targeting of rod and cone photoreceptors with a human rhodopsin kinase promoter. *Invest. Ophthalmol. Vis. Sci.*, **48**, 3954–3961.
24. Aartsen, W.M., Kantardzhieva, A., Klooster, J., van Rossum, A.G., van de Pavert, S.A., Versteeg, I., Cardozo, B.N., Tonagel, F., Beck, S.C., Tanimoto, N. *et al.* (2006) Mpp4 recruits Psd95 and Veli3 towards the photoreceptor synapse. *Hum. Mol. Genet.*, **15**, 1291–1302.
25. Stohr, H., Heisig, J.B., Benz, P.M., Schoberl, S., Milenkovic, V.M., Strauss, O., Aartsen, W.M., Wijnholds, J., Weber, B.H. and Schulz, H.L. (2009) TMEM16B, a novel protein with calcium-dependent chloride channel activity, associates with a presynaptic protein complex in photoreceptor terminals. *J. Neurosci.*, **29**, 6809–6818.
26. Aartsen, W.M., Arsanto, J.P., Chauvin, J.P., Vos, R.M., Versteeg, I., Cardozo, B.N., Le Bivic, A. and Wijnholds, J. (2009) PSD95beta regulates plasma membrane Ca2+ pump localization at the photoreceptor synapse. *Mol. Cell Neurosci.*, **41**, 156–165.
27. Dalkara, D., Kolstad, K.D., Guerin, K.I., Hoffmann, N.V., Visel, M., Klimczak, R.R., Schaffer, D.V. and Flannery, J.G. (2011) AAV mediated GDNF secretion from retinal glia slows down retinal degeneration in a rat model of retinitis pigmentosa. *Mol. Ther.*, **19**, 1602–1608.
28. Klimczak, R.R., Koerber, J.T., Dalkara, D., Flannery, J.G. and Schaffer, D.V. (2009) A novel adeno-associated viral variant for efficient and selective intravitreal transduction of rat Muller cells. *PLoS ONE*, **4**, e7467.
29. Rowan, S. and Cepko, C.L. (2004) Genetic analysis of the homeodomain transcription factor Chx10 in the retina using a novel multifunctional BAC transgenic mouse reporter. *Dev. Biol.*, **271**, 388–402.
30. Malicki, J. and Driever, W. (1999) oko meduzy mutations affect neuronal patterning in the zebrafish retina and reveal cell-cell interactions of the retinal neuroepithelial sheet. *Development*, **126**, 1235–1246.
31. Park, B., Alves, C.H., Lundvig, D.M., Tanimoto, N., Beck, S.C., Huber, G., Richard, F., Klooster, J., Andlauer, T.F., Swindell, E.C. *et al.* (2011) PALS1 Is Essential for Retinal Pigment Epithelium Structure and Neural Retina Stratification. *J. Neurosci.*, **31**, 17230–17241.
32. Cho, S.H., Kim, J.Y., Simons, D.L., Song, J.Y., Le, J.H., Swindell, E.C., Jamrich, M., Wu, S.M. and Kim, S. (2012) Genetic ablation of Pals1 in retinal progenitor cells models the retinal pathology of Leber congenital amaurosis. *Hum. Mol. Genet.*, **21**, 2663–2676.
33. Reese, B.E. (2011) Development of the retina and optic pathway. *Vision Res.*, **51**, 613–632.
34. van de Pavert, S.A., Sanz, A.S., Aartsen, W.M., Vos, R.M., Versteeg, I., Beck, S.C., Klooster, J., Seeliger, M.W. and Wijnholds, J. (2007) Crb1 is a determinant of retinal apical Muller glia cell features. *Glia*, **55**, 1486–1497.
35. Omori, Y. and Malicki, J. (2006) oko meduzy and related crumbs genes are determinants of apical cell features in the vertebrate embryo. *Curr. Biol.*, **16**, 945–957.
36. Hsu, Y.C., Willoughby, J.J., Christensen, A.K. and Jensen, A.M. (2006) Mosaic Eyes is a novel component of the Crumbs complex and negatively regulates photoreceptor apical size. *Development*, **133**, 4849–4859.
37. den Hollander, A.I., Heckenlively, J.R., van den Born, L.I., de Kok, Y.J., van der Velde-Visser, S.D., Kellner, U., Jurklies, B., van Schooneveld, M.J., Blankenagel, A., Rohrschneider, K. *et al.* (2001) Leber congenital amaurosis and retinitis pigmentosa with Coats-like exudative vasculopathy are associated with mutations in the crumbs homologue 1 (CRB1) gene. *Am. J. Hum. Genet.*, **69**, 198–203.
38. den Hollander, A.I., Roepman, R., Koenekoop, R.K. and Cremers, F.P. (2008) Leber congenital amaurosis: genes, proteins and disease mechanisms. *Prog. Retin. Eye Res.*, **27**, 391–419.
39. Gosens, I., den Hollander, A.I., Cremers, F.P. and Roepman, R. (2008) Composition and function of the Crumbs protein complex in the mammalian retina. *Exp. Eye Res.*, **86**, 713–726.
40. van den Hurk, J.A., Rashbass, P., Roepman, R., Davis, J., Voesenek, K.E., Arends, M.L., Zonneveld, M.N., van Roekel, M.H., Cameron, K., Rohrschneider, K. *et al.* (2005) Characterization of the Crumbs homolog 2 (CRB2) gene and analysis of its role in retinitis pigmentosa and Leber congenital amaurosis. *Mol. Vis.*, **11**, 263–273.
41. Clapcote, S.J. and Roder, J.C. (2005) Simplex PCR assay for sex determination in mice. *Biotechniques*, **38**, 702, 704, 706.
42. Tanimoto, N., Muehlfriedel, R.L., Fischer, M.D., Fahl, E., Humphries, P., Biel, M. and Seeliger, M.W. (2009) Vision tests in the mouse: Functional phenotyping with electroretinography. *Front. Biosci.*, **14**, 2730–2737.
43. Seeliger, M.W., Beck, S.C., Pereyra-Munoz, N., Dangel, S., Tsai, J.Y., Luhmann, U.F., van de Pavert, S.A., Wijnholds, J., Samardzija, M., Wenzel, A. *et al.* (2005) In vivo confocal imaging of the retina in animal models using scanning laser ophthalmoscopy. *Vis. Res.*, **45**, 3512–3519.
44. Hermens, W.T., ter Brake, O., Dijkhuizen, P.A., Sonnemans, M.A., Grimm, D., Kleinschmidt, J.A. and Verhaagen, J. (1999) Purification of recombinant adeno-associated virus by iodixanol gradient ultracentrifugation allows rapid and reproducible preparation of vector stocks for gene transfer in the nervous system. *Hum. Gene Ther.*, **10**, 1885–1891.
45. Hellstrom, M., Ruitenberg, M.J., Pollett, M.A., Ehlert, E.M., Twisk, J., Verhaagen, J. and Harvey, A.R. (2009) Cellular tropism and transduction properties of seven adeno-associated viral vector serotypes in adult retina after intravitreal injection. *Gene Ther.*, **16**, 521–532.
46. Koerber, J.T., Klimczak, R., Jang, J.H., Dalkara, D., Flannery, J.G. and Schaffer, D.V. (2009) Molecular evolution of adeno-associated virus for enhanced glial gene delivery. *Mol. Ther.*, **17**, 2088–2095.
47. Blits, B., Derks, S., Twisk, J., Ehlert, E., Prins, J. and Verhaagen, J. (2010) Adeno-associated viral vector (AAV)-mediated gene transfer in the red nucleus of the adult rat brain: comparative analysis of the transduction properties of seven AAV serotypes and lentiviral vectors. *J. Neurosci. Methods*, **185**, 257–263.
48. Brummelkamp, T.R., Bernards, R. and Agami, R. (2002) A system for stable expression of short interfering RNAs in mammalian cells. *Science*, **296**, 550–553.